ARTICLES
https://doi.org/10.1038/s41590-019-0467-1
nature immunology

IL-1R3 blockade broadly attenuates the functions of six members of the IL-1 family, revealing their contribution to models of disease

Jesper Falkesgaard Højen[1,2,3], Marie Louise Vindvad Kristensen[3], Amy S. McKee[3,4], Megan Taylor Wade[3], Tania Azam[3], Lars P. Lunding[5], Dennis M. de Graaf[3,6], Benjamin J. Swartzwelter[3], Michael Wegmann[5], Martin Tolstrup[1,2], Karsten Beckman[7], Mayumi Fujita[4,8], Stephan Fischer[7] and Charles A. Dinarello[3,6*]

Interleukin (IL)-1R3 is the co-receptor in three signaling pathways that involve six cytokines of the IL-1 family (IL-1α, IL-1β, IL-33, IL-36α, IL-36β and IL-36γ). In many diseases, multiple cytokines contribute to disease pathogenesis. For example, in asthma, both IL-33 and IL-1 are of major importance, as are IL-36 and IL-1 in psoriasis. We developed a blocking monoclonal antibody (mAb) to human IL-1R3 (MAB-hR3) and demonstrate here that this antibody specifically inhibits signaling via IL-1, IL-33 and IL-36 in vitro. Also, in three distinct in vivo models of disease (crystal-induced peritonitis, allergic airway inflammation and psoriasis), we found that targeting IL-1R3 with a single mAb to mouse IL-1R3 (MAB-mR3) significantly attenuated heterogeneous cytokine-driven inflammation and disease severity. We conclude that in diseases driven by multiple cytokines, a single antagonistic agent such as a mAb to IL-1R3 is a therapeutic option with considerable translational benefit.

Inhibition of cytokine function is a cornerstone of many clinical interventions. Although treatment often focuses on blocking either a single ligand or its primary receptor[1], targeting a single cytokine can imply that a disease is due to a distinct mediator. However, this is not always the case. The heterogeneous nature of inflammatory diseases may explain less than optimal outcomes or failures in clinical trials when neutralizing only a single cytokine, in particular, when preclinical models reveal synergy of two cytokines. Diseases where more than one IL-1 family member has been attributed a prominent role, such as IL-1β and IL-33 in asthma[2,3] and IL-1α and IL-36 in psoriasis[4,5], this heterogeneity. Because there is a basal inflammatory component in most diseases, blockade of the specific disease-driving cytokine as well as the inflammatory component would therefore probably improve outcomes.

The IL-1 family consists of 11 members, with a role in innate inflammation and acquired immunity[6]. In the search for an improved druggable target in the IL-1 family, we assessed possible interventional sites. The receptor family consists of ten members and one binding protein (IL-18BP)[7]. Of these, IL-1R1 binds IL-1α and IL-1β, recruiting IL-1R3 to form the trimeric signaling complex. IL-1R4 (ST2) binds IL-33 and forms a trimeric complex with IL-1R3, and IL-1R6 binds IL-36α, IL-36β and IL-36γ, similarly recruiting IL-1R3. In each case, IL-1R3 is the co-receptor that allows for the dimerization of the cytoplasmic Toll/IL-1R domains, triggering a unique response[8,9]. With IL-1R3 being the signaling regulator for six different cytokines, there are IL-1R3-dependent cytokines inducing inflammation, a type 1 helper T cell (T_H1) response, a type 2 helper T cell (T_H2) response or a combination of inflammation with either T_H1 or T_H2 responses. Blocking a common co-receptor, rather than individual primary receptors or ligands, may therefore provide a new mode of action for reducing associated diseases.

We describe here a fully humanized blocking mAb targeting human IL-1R3 (MAB-hR3), with an incorporated Fc-LALA (L234A/L235A) substitution to prevent the triggering of FcγRs[10,11]. We determined direct in vitro inhibition of signaling through IL-1R1, IL-1R4 and IL-1R6 by this mAb and investigated the inflammatory contribution of the IL-1R3 signaling-associated cytokines. Additionally, we conducted proof-of-concept in vivo studies using a mouse IL-1R3 mAb (MAB-mR3) in models of IL-1β-dependent monosodium urate crystal (MSU) peritonitis, IL-33-dependent ovalbumin (OVA) allergic airway inflammation and IL-36-dependent imiquimod (IMQ)-induced psoriasis. In each case, IL-1R3 blockade proved effective in attenuating the disease phenotypes.

Results

MAB-hR3 binds dose-dependently, specifically and with high affinity to human IL-1R3. We initially examined the binding properties of MAB-hR3. MAB-hR3 is a humanized IgG1 Fc-LALA substituted IL-1R3 mAb, produced in wild-type albino zika rabbits. We observed dose-dependent binding to an IL-1R3-expressing human melanoma cell line, SK-MEL-30 (half-maximum effective concentration (EC_{50}) = 274 ng ml^{-1}, K_d = 1.73 nM, assuming complete specific binding Fig. 1a). Comparing MAB-hR3 to an IgG isotype control on both the human SK-MEL-30 cell line (Fig. 1b) and the

[1]Department of Infectious Diseases, Aarhus University Hospital, Aarhus, Denmark. [2]Department of Clinical Medicine, Aarhus University, Aarhus, Denmark. [3]Department of Medicine, University of Colorado Denver, Aurora, CO, USA. [4]Department of Microbiology and Immunology, University of Colorado Denver, Aurora, CO, USA. [5]Division of Asthma Exacerbation & Regulation, Priority Area Asthma and Allergy, Leibniz Lung Center Borstel, Airway Research Center North (ARCN), Member of the German Center for Lung Research (DZL), Borstel, Germany. [6]Department of Internal Medicine, Radboud University Medical Center, Nijmegen, the Netherlands. [7]MAB Discovery GmbH, Neuried, Germany. [8]Department of Dermatology, University of Colorado Denver, Aurora, CO, USA. *e-mail: cdinare333@aol.com

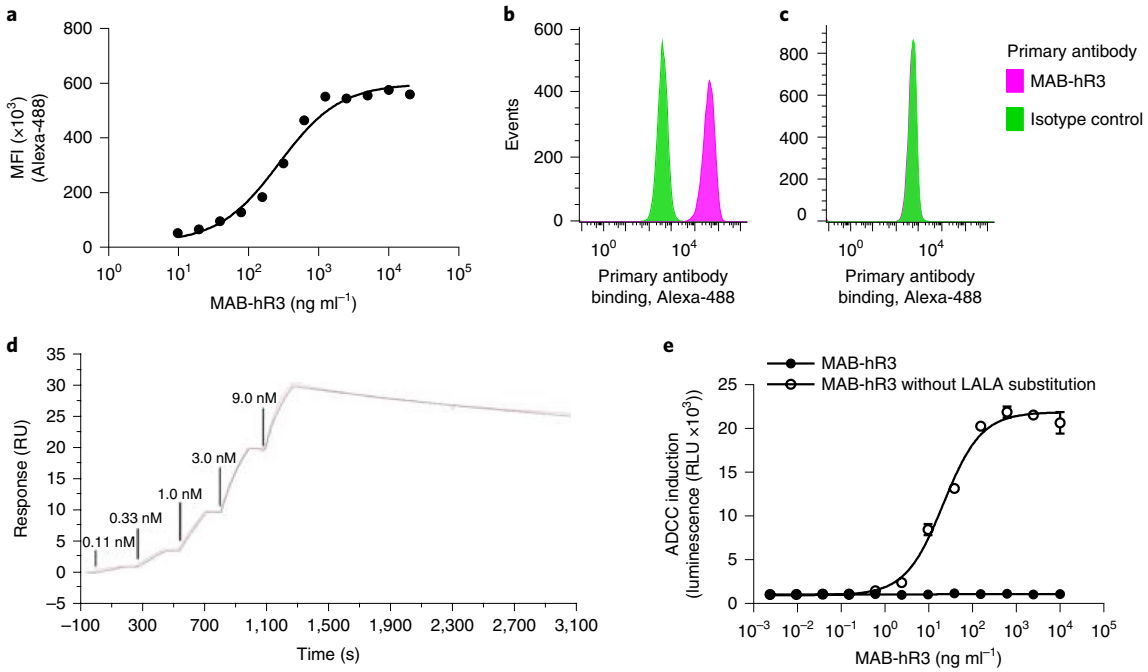

Measurement	k_a ($M^{-1}s^{-1}$)	k_d (s^{-1})	K_d (M)	R_{max}
1	5.14×10^5	2.07×10^{-4}	4.0×10^{-10}	46.6 RU
2	5.31×10^5	2.27×10^{-4}	4.3×10^{-10}	48.3 RU
Mean:	5.23×10^5	2.17×10^{-4}	4.2×10^{-10}	47.5 RU

Fig. 1 | MAB-hR3 binds dose-dependently and with high affinity to IL-1R3. a, Dose-dependent binding of MAB-hR3 (using fluorescence-activated cell sorting analysis) to the IL-1R3-expressing human cell line, SK-MEL-30 (represented as mean fluorescence intensity (MFI)). **b**,**c**, Fluorescence-activated cell sorting analysis of MAB-hR3 binding to the IL-1R3-expressing human cell line, SK-MEL-30 (**b**) and the murine cell line, NIH-3T3 (**c**) (isotype control included). **d**, MAB-hR3 kinetics analyzed using surface plasmon resonance (one measurement depicted). Single-cycle kinetics were performed using increasing concentrations of hIL-1R3 (0.111–9 nM). R_{max}, maximum response; RU, resonance units. **e**, The impact of the incorporated MAB-hR3 LALA substitution on binding to FcγRIIIa as measured by NFAT reporter gene activation in an ADCC luciferase reporter bioassay (Jurkat effector cells). RLU, relative luciferase units. Data are from one representative experiment (**a**–**d**) confirmed once with similar results and show the mean ± s.e.m. from four technical replicates (**e**).

murine cell line NIH-3T3 (Fig. 1c), we observed species specificity and ruled out nonspecific binding (gating strategy Supplementary Fig. 1a).

Next, we demonstrated that MAB-hR3 binds human IL-1R3 using immunoprecipitation. MAB-hR3 was incubated with A549 cell lysates, immunoprecipitated and subjected to analysis by mass spectrometry. We confirmed the presence of IL-1R3 peptides in the MAB-hR3 immunoprecipitation (Supplementary Fig. 1b), whereas no IL-1R3 peptides were observed using an IgG isotype control (data not shown), as we did not observe nonspecific binding of MAB-hR3 to any common sequence of IL-1 family receptors that share homologous IgG domains. The data observed when using MAB-hR3 could not be due to specific binding of multiple IL-1 family receptors simultaneously, but rather IL-1R3-specific effects. Formal binding kinetics for MAB-hR3 to human IL-1R3 were established using surface plasmon resonance (K_d = 415 pM) (Fig. 1d).

MAB-hR3 has an incorporated double substitution, LALA that significantly reduces binding to FcγRs[10]. This was confirmed in an antibody-dependent cellular cytotoxicity (ADCC) bioassay, measuring NFAT activation in FcγRIIIa expressing Jurkat effector cells

Fig. 2 | MAB-hR3 inhibits IL-1R1, IL-1R4 and IL-1R6 signaling in vitro and is functional ex vivo. a–**c**, Suppression of cytokine signaling by MAB-hR3 compared to polyclonal goat-anti-IL-1R3. **a**, Inhibition of IL-1α signaling in an A549 luciferase reporter cell line (NF-κB activation) (IC_{50}(MAB-hR3) = 146 ng ml^{-1}; IC_{50}(polyclonal) = 2,609 ng ml^{-1}; $P < 0.0001$). **b**, IL-33 signaling inhibition in an HEK293 SEAP reporter cell line (NF-κB/AP-1 activation) (IC_{50}(MAB-hR3) = 749 ng ml^{-1};IC_{50}(polyclonal) = 20,986 ng ml^{-1}; $P < 0.0001$). **c**, IL-36γ signaling inhibition in a HEK293/17 luciferase reporter cell line (NF-κB activation) (IC_{50}(MAB-hR3) = 17.1 ng ml^{-1}; IC_{50}(polyclonal) = 769 ng ml^{-1}; $P < 0.0001$). **d**–**f**, Comparison of cytokine production by MAB-hR3 to IL-1Ra. **d**, IL-1α-induced IL-6 production in a human lung epithelial cell line (A549). **e**, IL-33-induced IL-8 production in a human mast cell line (HMC-1). **f**, IL-36α-induced IL-8 production in a human keratinocytic cell line (HaCaT). **g**, The levels of soluble receptors in whole-blood cultures after 24 h of incubation in media. **h**,**i**, Heat-killed (hk) *C. albicans* stimulation (0.5×10^6 ml^{-1}, 24 h) of IL-17 and IL-6 production in whole-blood cultures. **j**, Preincubation (14 h) of MAB-hR3 (1 μg ml^{-1}) with recombinant sIL-1R3 in increasing concentrations, before evaluating IL-6 production in hk *C. albicans*-stimulated whole blood. **k**, The anti-inflammatory effect of various concentrations of sIL-1R3 alone in hk *C. albicans*-stimulated whole blood. UT, untreated. IL-1Ra, 10 μg ml^{-1}, 578 nM; MAB-hR3, 10 μg ml^{-1}, 69 nM. Inhibitors compared to stimulation alone. *$P < 0.05$, **$P < 0.01$ (paired two-sided Student's *t*-test). Data shown are mean ± s.e.m and are from one representative experiment (**a**–**c**) confirmed once with similar results, $n = 3$ independent experiments (**d**–**f**), $n = 11$ (**g**), $n = 10$ (**h**,**i**) and $n = 9$ (**j**,**k**) donors.

as a readout of FcR triggering. Here, MAB-hR3 with and without the incorporated mutation were compared (Fig. 1e). We observed that the LALA mutation completely abrogated FcγR-dependent activation of the NFAT reporter, indicating a lack of cytotoxic potential. In line with this, incubating MAB-hR3 (1 μg ml^{-1} or 20 μg ml^{-1}) with peripheral blood mononuclear cells (PBMCs) did not reveal any significant change in a WST-1 cell proliferation assay compared to control. Also, we did not observe an increase in IL-6 production as an indication of Fc-mediated agonistic properties (Supplementary Fig. 1c,d)[12,13].

MAB-hR3 inhibits signaling for IL-1R1, IL-R4 and IL-R6. We evaluated the ability of MAB-hR3 to inhibit signaling through the three IL-1R3-associated ligand binding receptors: IL-1R1, IL-1R4 and IL-1R6. For each pathway, we used modified gene-reporter cell lines expressing the receptor of interest comparing to a polyclonal IL-1R3-blocking antibody. To determine IL-1R1 signaling interference using IL-1R3 blockade, we used IL-1α stimulation of an A549 luciferase reporter cell line measuring nuclear factor (NF)-κB activation (IC_{50}(MAB-hR3) = 146 ng ml^{-1}; Fig. 2a). For IL-1R4, we used IL-33 stimulation of a HEK293 SEAP reporter cell line

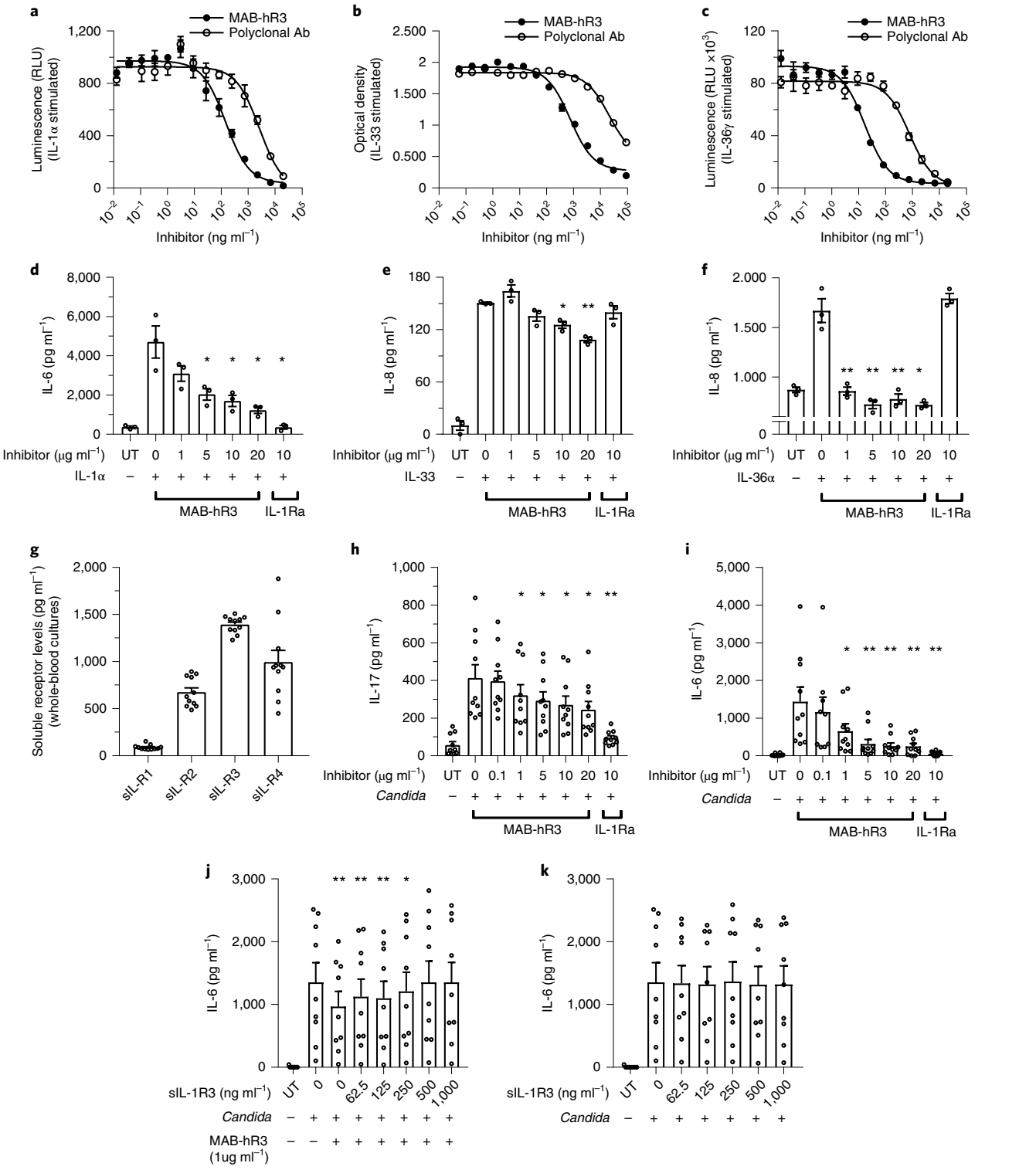

(NF-κB/AP-1 activation; IC_{50}(MAB-hR3) = 749 ng ml^{-1}; Fig. 2b). Lastly, IL-1R6 interference was investigated using IL-36γ stimulation of a HEK293/17 luciferase reporter cell line (NF-κB activation; IC_{50}(MAB-hR3) = 17.1 ng ml^{-1}; Fig. 2c). Significant inhibition was observed in each of the three assays at low concentrations.

Next, we evaluated the inhibition of cytokine production from cells lines without reporter modifications. We used MAB-hR3 concentrations ranging from 1 μg ml^{-1} (6.9 nM) to 20 μg ml^{-1} (138 nM). We used native A549 cells for IL-1α-induced IL-6 production, a human mast cell line (HMC-1) for IL-33-induced IL-8 production and a human keratinocyte cell line (HaCaT) for IL-36α-induced IL-8 production.

In the A549, HMC-1 and HaCaT cell lines, MAB-hR3 decreased cytokine production significantly by up to 74% (IL-6), 28% (IL-8) and 57% (IL-8), respectively (Fig. 2d–f). MAB-hR3 showed a clear dose-dependent inhibitory response in both A549 and HMC-1 cells; however, it inhibited with similar efficacy at each concentration used in HaCaT cells. To verify the influence of IL-1 signaling in these cell lines, we also examined IL-1Ra (anakinra) as an inhibitor. We used a concentration of IL-1Ra (10 μg ml^{-1} (578 nM)), which is tenfold greater than the maximum blood level in patients with rheumatoid arthritis treated with a standard clinical dose of 100 mg subcutaneously. IL-1Ra had a statistically significant impact on IL-1α-induced IL-6 production in A549 cells (92% decrease), whereas no significant reductions were observed on IL-33 nor IL-36α-induced IL-8 production, underlining that the effect of MAB-hR3 in these cell lines was not related to the inhibition of IL-1R1 signaling.

Binding of soluble IL-1R3 does not abrogate the anti-inflammatory effects of MAB-hR3. IL-1R3 is found in a soluble form (sIL-1R3) in the circulation where it increases the neutralization capacity of IL-1R2. IL-1β binds to the soluble decoy receptor, IL-1R2 (sIL-1R2). When sIL-1R3 binds to this complex, the affinity to bind IL-1β increases by ~100-fold[14]. Hence, sIL-1R3 functions as an anti-inflammatory receptor. In the circulation, there is an excess amount of sIL-1R3 (approximately 300 ng ml^{-1} in plasma) compared to sIL-1R2 (approximately 7 ng ml^{-1} in plasma)[14], both beyond the circulating levels of IL-1β (mean level of 0.33 pg ml^{-1} in 500 healthy subjects[15]).

To determine whether MAB-hR3 would affect the anti-inflammatory function of sIL-1R3, we used whole-blood cultures to mimic the conditions of MAB-hR3 infusions in humans. We initially confirmed the presence of sIL-1R1, sIL-1R2, sIL-1R3 and sIL-1R4 (Fig. 2g). Using heat-killed *Candida albicans* to mimic an inflammatory condition via dectin-1 receptor and Toll-like receptor 2 (refs. [16,17]), we measured IL-17 and IL-6 levels in the presence of MAB-hR3. Suppression of IL-17 and IL-6 production by MAB-hR3 takes place in whole-blood cultures containing sIL-1R3 (Fig. 2h,i). The importance of IL-1 in these cultures is illustrated by the ability of IL-1Ra to reduce IL-17 and IL-6 production by 77% and 96%, respectively. We conclude that any neutralization of endogenous sIL-1R3 by MAB-hR3 does not significantly impair the IL-1-blocking mechanism of soluble or cell-bound IL-1R2 in a complex with sIL-1R3.

We further evaluated the impact of MAB-hR3 on IL-1-dependent IL-6 production. We preincubated a fixed concentration of MAB-hR3 with increasing concentrations of recombinant sIL-1R3, to 'decoy' MAB-hR3 to bind to sIL-1R3. Increasing concentrations of sIL-1R3 did, in fact, reduce the inhibitory effect of MAB-hR3 as measured by IL-6 production (Fig. 2j). However, as there was no effect on *C. albic*ans-induced IL-6 production in the presence of increasing concentrations of recombinant sIL-1R3 alone (Fig. 2k), the decreased effect of MAB-hR3 was due to freely available antibody and not an anti-inflammatory function of sIL-1R3 itself. We conclude that although MAB-hR3 can be 'decoyed' to sIL-1R3, MAB-hR3 retains its ability to block IL-1R3 surface receptors and provides a robust reduction in inflammation.

Blocking IL-1R3 reduces monosodium urate crystal-mediated peritonitis. In order to study the effects of blocking IL-1R3 in models of human disease, we developed a chimeric mouse IgG2a Fc-LALA substituted IL-1R3 mAb (MAB-mR3), using wild-type albino zika rabbits for immunization. We used surface plasmon resonance to confirm the development of a high-affinity antibody (K_d = 63 pM), as well as functional testing and comparison to MAB-hR3 (Supplementary Fig. 2).

We sought to address the differences of IL-1R3 blockade compared to IL-1R1 blockade. The clinically established treatments of the IL-1R1 signaling pathway, and the importance of IL-1 in the development of comorbidities justified this comparison. Thus, we administered the antibody to mice challenged with MSU crystal-induced peritonitis, a model highly dependent on IL-1β[18]. Notably, this model also possesses some of the multifaceted interactions that take place in an acute gout attack, including morphological similarities between the synovium and peritoneal lining[19]. Animal models using MSU as well as humans with recurrent gout attacks respond dramatically to IL-1β blocking therapies[18–20].

In MSU-induced peritonitis, the inflammation is due to a white blood cell (WBC) influx to the peritoneal cavity. We observed a marked decrease in the total number of WBCs in the MAB-mR3-treated group compared to the vehicle-treated group (Fig. 3a). The decrease was consistent across multiple cell types: granulocytes (65% decrease), monocytes (57% decrease) and lymphocytes (42% decrease) (Fig. 3c). In the IL-1Ra-treated group, we observed a similar pattern, although less pronounced compared to that observed in the MAB-mR3-treated mice. In addition, protein concentration in the intraperitoneal (IP) fluid was evaluated as a marker of plasma protein leak, corresponding to the intensity of inflammation. Here, we observed no significant changes in any of the treatment groups (Fig. 3b).

We compared the levels of IL-1β in the peritoneal WBC lysates from MSU-treated mice. In the MAB-mR3-treated group, the mean IL-1β concentration level was 69% lower than in vehicle-treated mice (Fig. 3d). The total IL-1β in cell lysates consisted of both IL-1β precursor and matured IL-1β. This indicated that the amount of both mature IL-1β and its precursor available for caspase-1-mediated release was significantly decreased in the MAB-mR3 group, but not in the IL-1Ra-treated mice. To evaluate whether this was solely related to cell frequencies, we calculated the levels of IL-1β per million WBCs. Here, we still observed significantly lower levels of IL-1β (34%) in the MAB-mR3-treated mice compared to the vehicle control group (Fig. 3e). In contrast, we did not observe a decrease of IL-1β per cell in the IL-1Ra-treated group. We observed a significant difference in intracellular IL-1β levels between MSU-recruited WBCs from MAB-mR3 compared to IL-1Ra-treated mice (53% difference; Fig. 3d), which was also observed when normalized to WBCs (47% difference; Fig. 3e). Together, these data show that IL-1R3 blockade is more effective in reducing inflammation compared to IL-1R1 blockade in the MSU-induced peritonitis model.

Neutrophils are important effectors in innate immunity, actively recruited in the early phases of an inflammatory response. Thus, the observed decrease in granulocyte influx could also reflect some of the challenges that can be faced when inhibiting innate cytokines. In gout, neutrophils are the most abundant cells, degranulating as the cell phagocytizes the urate crystals. Here, the granule enzymes intensify inflammation and are damaging to tissues[21,22]. In line with this, we observed a significant increase in the concentration of elastase in the IP fluid from MSU-injected mice compared to saline-injected mice. In the mice exposed to MSU, MAB-mR3 significantly decreased IP fluid elastase by 48% (Fig. 3f). Further, elastase concentrations in IP cell lysates from MSU-injected mice decreased by 72% in the MAB-mR3 group, and by 50% in the IL-1Ra group (Fig. 3g). IP cell lysate myeloperoxidase (MPO) levels decreased by 68% in the MAB-mR3-treated group and by 51% in the IL-1Ra-treated group compared to vehicle controls (Fig. 3h).

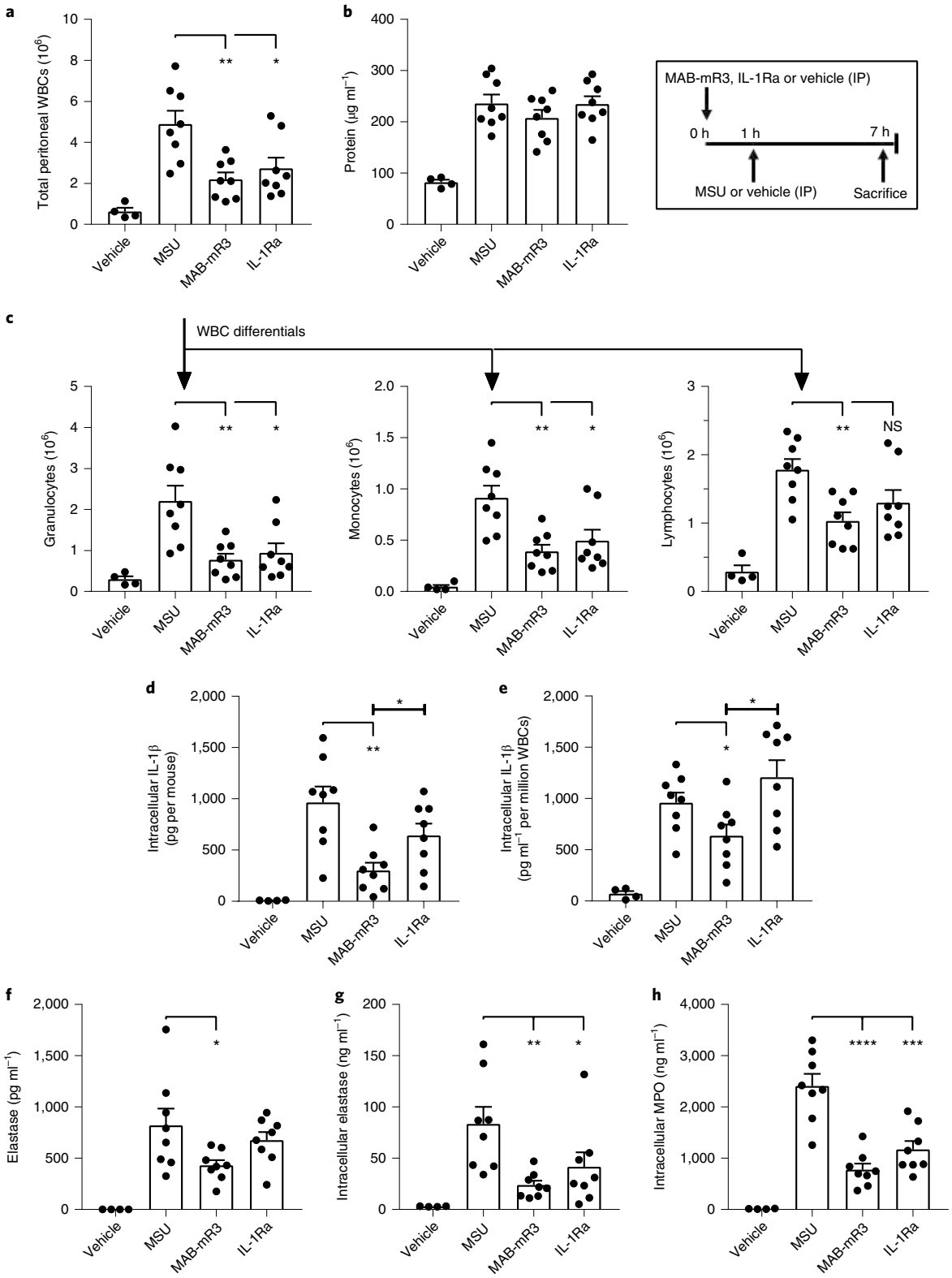

Fig. 3 | MAB-mR3 reduces in vivo MSU crystal-mediated peritonitis. a, Total WBC count from the peritoneal cavity (IP fluid). **b**, Protein concentration in IP fluid. **c**, Differential cell counts from (**a**) total cell influx. (NS, not significant $P = 0.07$). **d**, Total levels per mouse of intracellular IL-1β in WBCs from IP fluid. **e**, Levels of intracellular IL-1β normalized per million. WBCs from IP fluid. **f**, Levels of the neutrophil protease, elastase, in IP fluid. **g**, Total levels of intracellular elastase in WBCs from IP fluid. **h**, Total levels of intracellular MPO in WBCs from IP fluid. Vehicle group, vehicle + vehicle ($n = 4$). MSU group, vehicle + MSU ($n = 8$). MAB-mR3 group, MAB-mR3 + MSU ($n = 8$). IL-1Ra group, IL-1Ra + MSU ($n = 8$). Comparisons between inhibitor-treated and MSU-stimulated groups (**a**–**h**) and between treatment groups (**d**,**e**). *$P < 0.05$, **$P < 0.01$, ***$P < 0.001$ and ****$P < 0.0001$ (two-sided Student's *t*-test). Data are mean ± s.e.m.

Table 1 | Local and systemic inflammation in MSU-mediated peritonitis

	Vehicle ($n=4$)	MSU stimulated ($n=8$)	MAB-mR3 ($n=8$)	IL-1Ra ($n=8$)
IP fluid				
IL-6 (pg ml^{-1})	Below detection	65.0 ± 14.9	19.8 ± 5.8 ($P=0.014$)	36.9 ± 14.4 ($P=0.164$)
G-CSF (pg ml^{-1})	5.0 (2.8–5.5)	77.7 (53.6–97.3)	6.6 (4.9–33.0) ($P=0.015$)	8.6 (7.5–17.8) ($P=0.005$)
CXCL-1 (pg ml^{-1})	2.3 ± 0.5	82.7 ± 15.9	38.4 ± 11.6 ($P=0.041$)	84.3. ± 31.9 ($P=0.965$)
CCL-2 (pg ml^{-1})	Below detection	62.5 ± 11.9	26.2 ± 3.6 ($P=0.011$)	74.2 ± 14.5 ($P=0.545$)
CCL-3 (pg ml^{-1})	1.2 ± 0.1	4.9 ± 0.8	3.6 ± 0.5 ($P=0.161$)	5.7 ± 0.9 ($P=0.545$)
Systemic				
IL-6 (pg ml^{-1}), plasma	5.0 ± 3.4	69.8 ± 19.4	22.7 ± 5.7 ($P=0.011$)	29.5 ± 8.5 ($P=0.078$)
G-CSF (pg ml^{-1}), plasma	294 ± 28.4	6,245 ± 1,055	3,544 ± 2,743 ($P=0.010$)	1,157 ± 639 ($P=0.003$)
CXCL-1 (pg ml^{-1}), WB	272 (243–719)	2,525 (2,178–2,730)	1,366 (811–1,889) ($P=0.065$)	2,269 (1,511–3,213) ($P=0.959$)
MPO (ng norm.), spleen	42.5 ± 7.6	145 ± 9.7	89.3 ± 11.4 ($P=0.002$)	106 ± 9.7 ($P=0.013$)
CXCL-1 (pg norm.), spleen	16.2 (13.3–39.3)	189 (161–205)	72.5 (49.6–140) ($P=0.010$)	157 (95.3–238) ($P=0.645$)

Cytokine and chemokine concentrations locally (IP fluid) and systemically. WB, lysed whole blood, norm., normalized mg^{-1} of protein in spleen. Vehicle group, vehicle + vehicle ($n=4$). MSU group, vehicle + MSU ($n=8$). MAB-mR3 group, MAB-mR3 + MSU ($n=8$). IL-1Ra group, IL-1Ra + MSU ($n=8$). Comparisons between inhibitor-treated and MSU-stimulated groups. Student's *t*-test (two-sided) with mean ± s.e.m., except G-CSF, CXCL-1 in WB and CXCL-1 in spleen; Mann–Whitney *U* test with median and interquartile range.

Granulocyte colony-stimulating factor (G-CSF), a neutrophil attractant and activator, and IL-6 are induced by MSU; however, both were reduced in the IP fluid from mice treated with MAB-mR3, whereas IL-1Ra did not significantly impact IL-6 levels (Table 1). Similar data were observed for the chemokines CXCL-1 (KC), CCL-2 (MCP-1) and CCL-3 (MIP-1α). All were increased by MSU, and were reduced following MAB-mR3 treatment, where CXCL-1 and CCL-2 reached statistical significance (Table 1). The IL-1Ra-treated group did not exhibit a decrease in any of the chemokines assessed. Also, circulating IL-6 and G-CSF elevated by MSU, were significantly decreased by both MAB-mR3 and IL-1Ra (Table 1). CXCL-1 in lysed whole blood seemed to decrease in the MAB-mR3 group but was unaffected in the IL-1Ra-treated group. Both MPO and CXCL-1 were significantly lowered in spleen lysates using MAB-mR3, whereas IL-1Ra was less effective and showed no impact on CXCL-1 (Table 1). Collectively, these data indicate a broader impact of IL-1R3 blockade compared to blocking IL-1R1 alone.

IL-1R3 blockade broadly inhibits cytokine production compared to single pathway inhibition. Having shown the efficacy of IL-1R3 blockade compared to IL-1R1 blockade in the MSU model, we next examined the differential impact of blocking either IL-1R3 (using MAB-hR3), IL-1R4 (using sIL-1R4 (sST2)) or IL-1R6 (using IL-36Ra). We used heat-killed *C. albicans* stimulations of freshly isolated PBMCs to address IL-6 and interferon (IFN)-γ production. We found that blocking IL-1R3, but not signaling of IL-33 (through IL-1R4) or IL-36 (through IL-1R6), decreased the production of IL-6 by 67% (Fig. 4a). In contrast, the production of IFN-γ was significantly inhibited by blocking each of the three receptors (Fig. 4b). Thus, blocking IL-1R3 compared to the inhibition of IL-33 or IL-36 signaling, revealed a wider impact of targeting IL-1R3. Yet, these data also revealed a clear importance of IL-33 and IL-36 signaling in the *C. albicans*-induced production of IFN-γ. Still, this dependency was not observed in the production of IL-6, where only IL-1R3 signaling was contributing.

We next used a two-way mixed leukocyte reaction (MLR) as an endogenous inducer of cytokines. During a 5-d co-culture of PBMCs from two unrelated healthy donors, multiple cytokines were produced allowing the dissection of differences between IL-1R1 and IL-1R3 signaling more broadly. We found that MAB-hR3 significantly decreased the production of IFN-γ, IL-13, IL-17, IL-22, TNF, IL-6 and IL-10 (Fig. 4c–i). In contrast, inhibition of IL-1α and IL-1β signaling by IL-1Ra impacted only four cytokines: IFN-γ, IL-17, IL-22 and IL-10 (Fig. 4c,e,f,i). Thus, blocking IL-1R3 provides broader anti-inflammatory effects compared to IL-1R1 blockade (IL-1Ra).

Anti-IL-1R3 ameliorates ovalbumin-induced inflammation in vivo. The wide anti-inflammatory effects of IL-1R3 blockade prompted investigations into other models of human disease. Thus, we examined the OVA-induced allergic airway inflammation model, known for its IL-33 dependency[23]. Mice were fully sensitized with OVA before being treated with MAB-mR3. As expected, the challenge of intratracheal OVA resulted in high numbers of WBCs in the lungs, as measured in the bronchoalveolar lavage (BAL) fluid (Fig. 5a). Here, MAB-mR3 treatment resulted in a 46% decrease in the number of WBCs infiltrating the lungs and a similar (46%) decrease in eosinophils (Fig. 5b). Likewise, we observed a decrease in the content of both alveolar macrophages and neutrophils, the latter being highly significant.

We repeated the model to include measures of BAL fluid cytokines, mucus production and airway responsiveness, using the same sensitization schedule, but with aerosolized OVA as the challenge. We observed a similar significant decrease in the influx of WBCs in the BAL fluid (50%) as in the first experiment. Further, we observed a significant 54% decrease of the BAL cytokine IL-4, whereas IL-5, IL-13, IL-6 and TNF all decreased (63%, 64%, 76% and 33%, respectively), but not significantly (Fig. 5c). Histology examination of the lungs confirmed the difference between OVA alone and blocking inflammation using MAB-mR3. The difference was evident on both infiltrating immune cells (stained with hematoxylin and eosin (H&E)), and the significant decrease in mucus producing goblet cells in the airways (stained with periodic acid-Schiff (PAS)) (Fig. 5d,e). Changes in airway responsiveness were assessed using a methacholine (MCh) provocation test. We found that MAB-mR3 significantly decreased airway resistance at both 25 mg ml^{-1}, 50 mg ml^{-1} and 100 mg ml^{-1} of MCh, respectively (Fig. 5f), and observed no significant differences between MAB-mR3-treated and vehicle mice at any dose of MCh. Thus, MAB-mR3 limits both inflammation and related functional measures in this disease model.

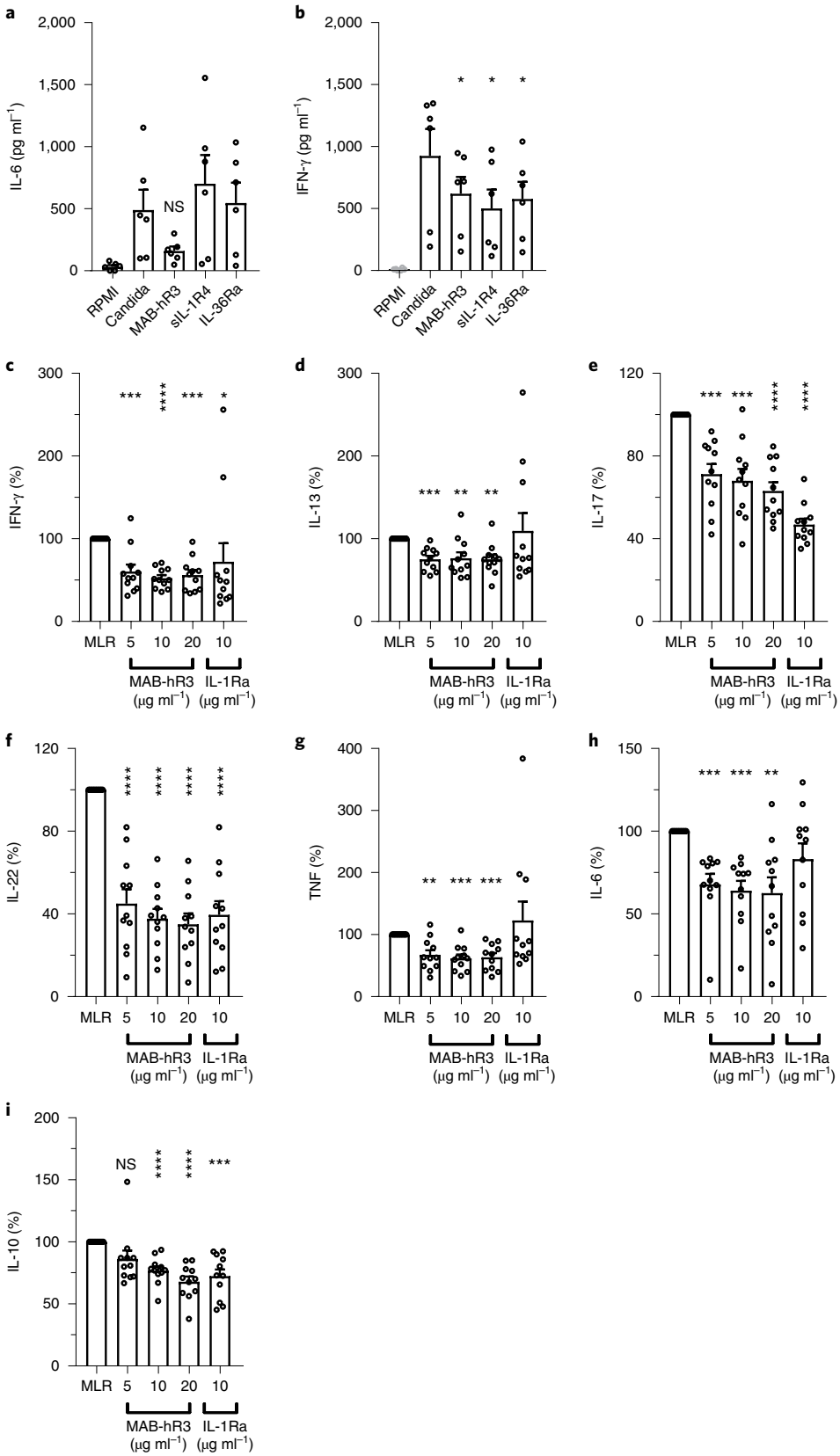

Fig. 4 | IL-1R3 blockade results in a broader anti-inflammatory phenotype compared to primary pathway inhibition. a,**b**, Inhibition of hk *C. albicans* (0.5×10^6 ml^{-1}, 24 h) induced IL-6 (**a**) or IFN-γ (**b**) production in PBMCs, using equal concentrations MAB-hR3, sIL-1R4 and IL-36Ra (69 nM) (NS, $P=0.052$). **c**–**i**, Percentage change in cytokines measured in the supernatants of two-way MLRs (5-d culture). MLR ranges are: IFN-γ (1.9–10.7 ng ml^{-1}), IL-13 (312–1,808 pg ml^{-1}), IL-17 (48.6–189 ng ml^{-1}), IL-22 (143–2,696 pg ml^{-1}), TNF (168–1,712 pg ml^{-1}), IL-6 (254–8,361 pg ml^{-1}) and IL-10 (107–1,302 pg ml^{-1}) (NS, $P=0.07$). Inhibitors compared to stimulation or MLR alone. *$P<0.05$, **$P<0.01$, ***$P<0.001$, ****$P<0.0001$ (paired two-sided Student's *t*-test). Data are mean + s.e.m and are from $n=6$ donors (**a**,**b**) and $n=11$ independent experiments (MLR, **c**–**i**). IL-1Ra, 10 μg ml^{-1}, 578 nM. MAB-hR3, 10 μg ml^{-1}, 69 nM.

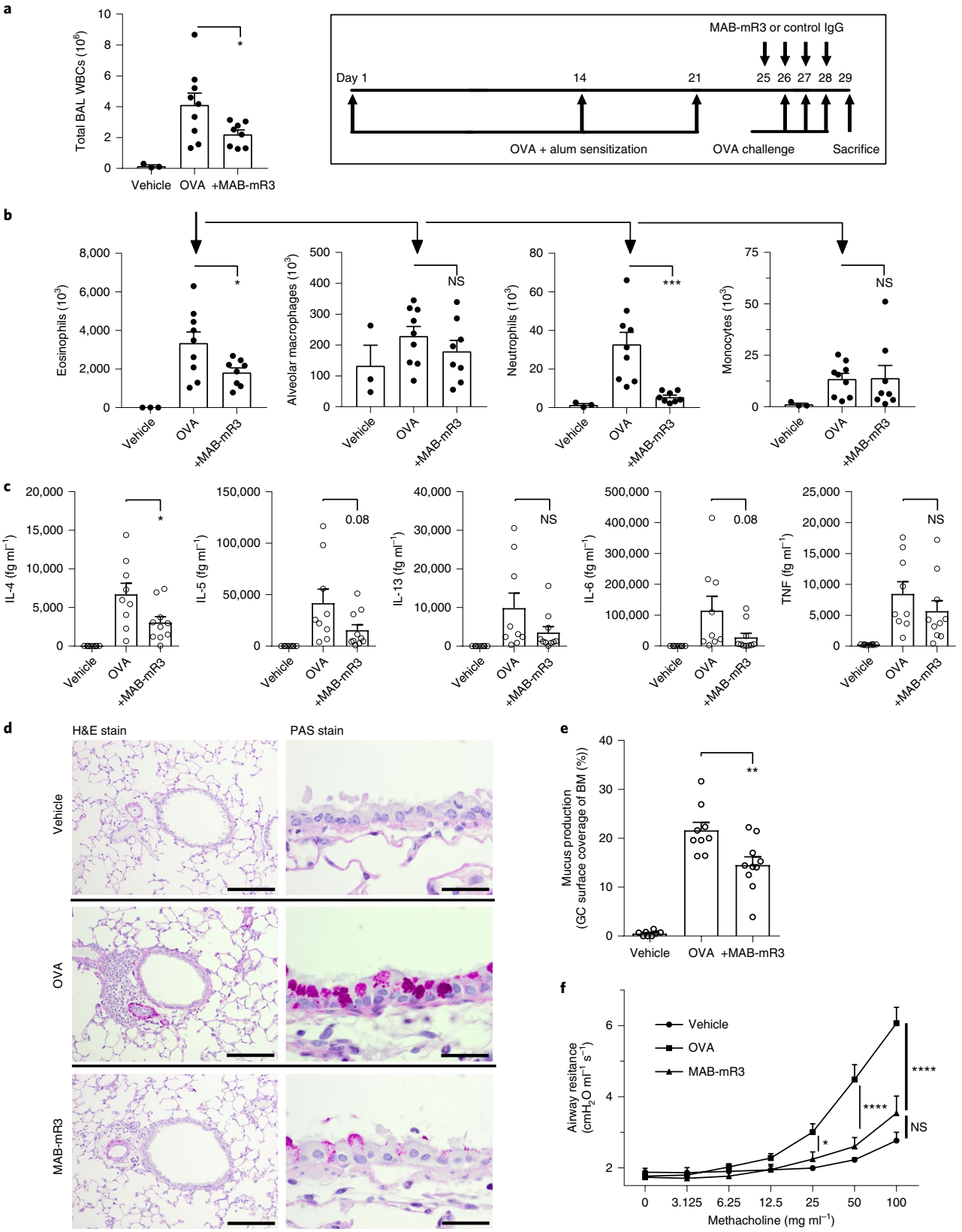

Fig. 5 | MAB-mR3 decreases OVA-induced allergic airway inflammation. a,**b**, Mice challenged by intranasal OVA (exp.1). $n=4$ (vehicle), $n=9$ (OVA) and $n=8$ (+MAB-mR3). **a**, Total WBCs from BAL fluid. **b**, Flow-defined cell differentials from **a**. **c**–**f**, Mice challenged by OVA aerosols (exp. 2). $n=8$ (vehicle), $n=9$ (OVA) and $n=10$ (+MAB-mR3) **c**, Cytokine measurements on BAL fluid. **d**, Cross sections from each interventional group using H&E (scale bar, 100 µm) and PAS (scale bar, 20 µm)-stained lung tissue, completed for each mouse with similar results. **e**, Area of airway epithelial basal membrane (BM) covered by goblet cells (GCs) (%). **f**, Airway resistance to increasing concentrations of MCh. (**a**–**c**,**e**), from $n=6$ (vehicle), $n=9$ (OVA) and $n=9$ (+MAB-mR3). Comparisons between MAB-mR3-treated mice and OVA alone (two-sided Student's *t*-test). **f**, Comparisons are shown between all groups at each concentration (Holm–Sidaks multiple comparisons test). $^*P<0.05$, $^{**}P<0.01$, $^{***}P<0.001$, NS, nonsignificant. Data show the mean + s.e.m.

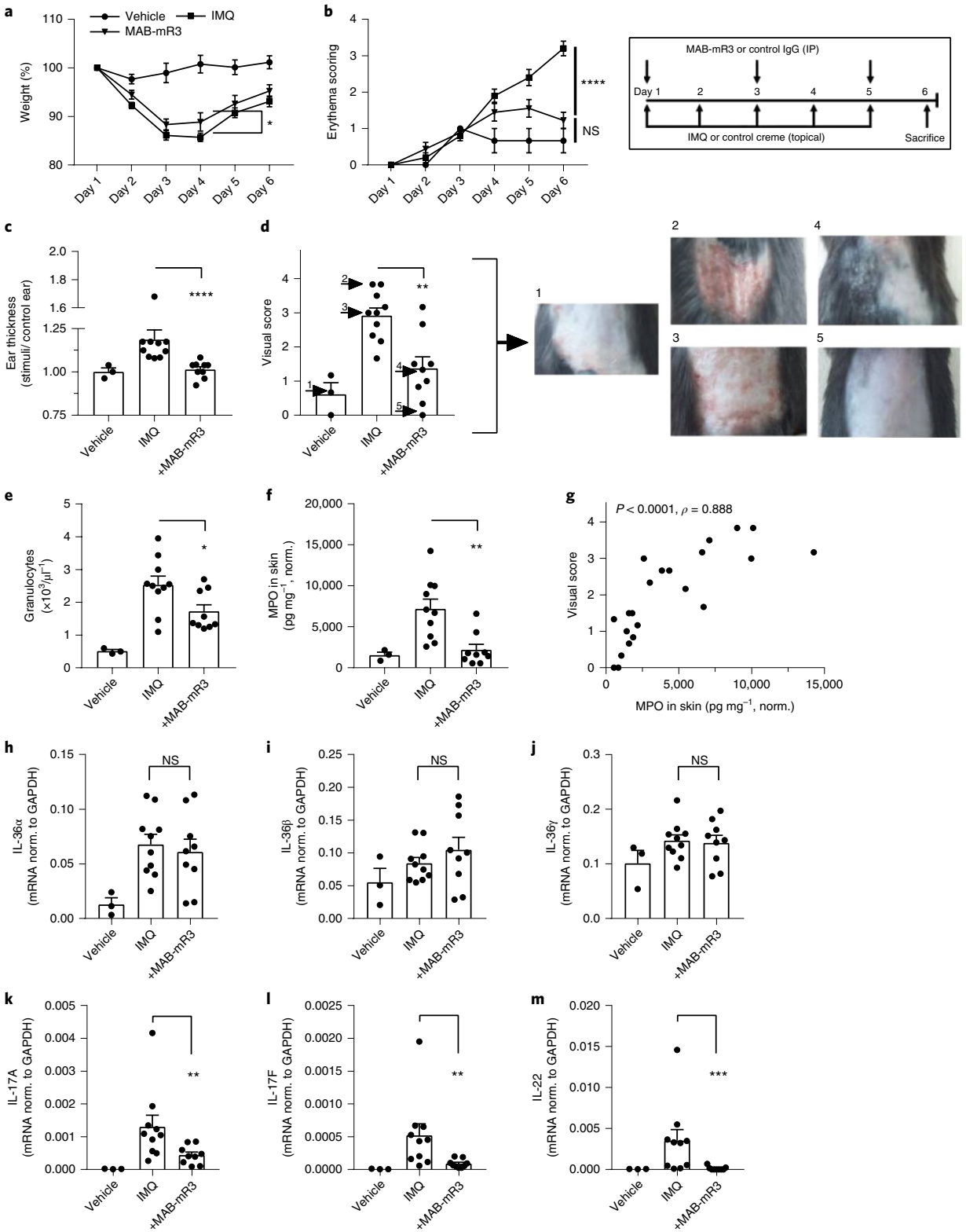

Fig. 6 | Improvement of imiquimod- induced psoriasis in vivo using MAB-mR3. a,**b**, Daily monitoring of (**a**) weight (percentage) and (**b**) erythema (scores: 0, unaffected; 4, maximum affected (unblinded)) throughout the experiment. **c**, Fold change in ear thickness between ears applied with IMQ and control cream on day 6. **d**, Visual scoring by six blinded people at the end of study (0, unaffected; 4, maximum affected (erythema and scaling)), arrow and number indicate depicted mice. **e**, Granulocyte concentrations in whole blood. **f**, MPO concentration in skin, normalized (norm.) per milligram of protein. **g**, Spearman correlation between data from **d** and **f**. **h**–**m**, mRNA expression of cytokines in back skin, normalized to glyceraldehyde 3-phosphate dehydrogenase (GAPDH) expression. Data are from $n=3$ (vehicle), $n=10$ (IMQ) and $n=9$ (+MAB-mR3) experiments. Comparisons of data (**c**–**m**) were between inhibitor-treated and IMQ-stimulated groups. Data were analyzed using (**a**,**b**) Holm–Sidaks multiple comparisons tests (all groups compared), a Mann–Whitney *U* test (**c**,**k**–**m**) and a Student's *t*-test (**d**–**f**,**h**–**j**). $^{*}P<0.05$, $^{**}P<0.01$, $^{***}P<0.001$, $^{****}P<0.0001$, NS, nonsignificant. Data shown represent the mean + s.e.m.

Anti-IL-1R3 ameliorates imiquimod-induced psoriasis attenuated in vivo. Mutations in IL-36Ra are linked to human pustular psoriasis[24,25]. Blocking the IL-36 signaling pathway through IL-1R3 could therefore alleviate this disease. We investigated MAB-mR3 in the IMQ-induced psoriasis mouse model[26]. We observed that the MAB-mR3-treated mice showed less weight loss compared to vehicle-treated IMQ-challenged mice (day 4) (Fig. 6a). Secondly, an unblinded erythema score revealed a significant difference on the last day of the experiment between MAB-mR3 and IMQ-mice (Fig. 6b). This anti-inflammatory effect was also observed in the ear thickness of mice receiving IMQ or vehicle cream on one ear, and control cream on the other. Here, we observed a striking difference between groups, with significantly less ear swelling (IMQ versus control) in the MAB-mR3-treated group (day 6) (Fig. 6c).

Next, skin inflammation for each mouse was scored by six individuals, each blinded to the treatment. The score was based on erythema, thickness and skin scaling (collective scale from 0–4, modified Psoriasis Area Severity Index). The MAB-mR3-treated group was graded with significantly lower scores than mice not receiving treatment (Fig. 6d, examples of scoring depicted). We similarly found the numbers of circulating granulocytes on the day of sacrifice were significantly fewer (32% decrease) in MAB-mR3-treated mice ($P = 0.03$) (Fig. 6e), but also the concentration of MPO in the skin was lower (69%) (Fig. 6f), indicative of lower numbers of neutrophils in the skin, less neutrophil degranulation or both. A clear correlation between the visual scores and the levels of MPO underlined the importance of these observations (Fig. 6g).

Lastly, we measured the transcriptional changes in the skin. We observed that topical application of IMQ significantly upregulated IL-36α mRNA levels in the skin, but not IL-36β or IL-36γ. MAB-mR3 treatment did not affect expression for either of the IL-36 subtypes (Fig. 6h–j). We also determined mRNA levels of IL-17a, IL-17f and IL-22, known key regulators in the pathogenesis of psoriasis. Here, we observed that blocking IL-1R3 using MAB-mR3 significantly decreased the transcription of all three cytokines: IL-17a (66%), IL-17f (83%) and IL-22 (96%). Thus, a single therapeutic intervention can markedly reduce multiple important mediators of disease, disclaiming the need for multiple cytokine interventions.

Discussion

Dysregulation of the innate immune system takes place in atherosclerosis, autoimmune diseases, Alzheimer's disease and cancer[27–30]. For example, a global trial of 10,000 patients at risk for a second heart attack or stroke revealed that specific neutralization of IL-1β reduced both atherosclerosis and heart failure, but also the incidence and survival of cancer[31,32]. Thus, innate inflammation can be reduced by lowering the level of IL-1β. Accordingly, our hypothesis was that blocking IL-1R3 could reduce both the specific cytokine of a disease, for example IL-33 in asthma, as well as the associated dysregulated IL-1 component driving basal inflammation, contributing not only to the disease phenotype, but also to the development of comorbidities.

In the present study, we addressed responses specific for IL-1, IL-33 and the IL-36 subfamily, and found that blocking IL-1R3 was highly effective in models of peritonitis, allergic airway inflammation and psoriasis. In each of these models, there was an inflammatory component from either IL-1β or IL-1α. In the case of MSU peritonitis, IL-1β was the primary disease-driving cytokine. In asthma or psoriasis, inflammation from IL-1 worsens the severity of the disease manifestation.

The initial in vitro data supported the rationale for examining the broad effects of IL-1R3 blockade in vivo. Since MSU-induced inflammation is primarily driven by IL-1β, IL-1Ra was used as the positive control for efficient IL-1R1 inhibition. Despite using a four-fold higher molar dose of IL-1Ra compared to MAB-mR3, blocking IL-1R3 provided an additional level of protection. We speculate that blockade of the alarmin effects of IL-33 in barrier cells[33], such as the peritoneal lining, might be of importance. IL-33 is traditionally known to induce T_H2-dominated inflammation. However, in both the peritoneal cavity and in the skin, IL-33 induces a predominant neutrophil milieu as observed here[34,35].

Caspase-1 inhibition can similarly be effective in MSU models[20]. However, extracellular cleavage of the IL-1β precursor by neutrophilic elastase and proteinase 3 can result in generation of active mature IL-1β[36,37]. Thus blocking IL-1 receptors is probably superior in diseases such as neutrophil-predominant arthritis, where elastase contributes substantially to IL-1β-driven inflammation[37]. In our MSU model, we observed a significant decrease in both granulocyte influx as well as elastase production when blocking IL-1R3 using MAB-mR3.

We next compared the effects of IL-1R3 blockade with that of specific IL-1R4 or IL-1R6 blockade. Here, we observed that T_H1 responses driven by IL-33 or IL-36 cytokines could be reduced by IL-1R3 blockade. Secondly, that blocking IL-1R3 had a broader anti-inflammatory effect compared to isolated IL-33 or IL-36 signaling inhibition, findings that were recapitulated when investigating the differences between IL-1R1 and IL-1R3 blockade using two-way MLRs. For that reason, we found cause to exploit the IL-1R3 blockade in diseases influenced by multiple IL-1 family members. For instance the highly IL-33-dependent OVA-induced allergic asthma model[38], as well as in the IL-36-dependent IMQ-induced psoriasis model[39].

In the airways, IL-33 promotes a T_H2 response, attracting eosinophils and basophils. MAB-mR3 treatment significantly reduced cell influx into the airways, primarily due to a marked decrease in eosinophils that are important in allergen-triggered airway inflammation[40]. We also observed a decrease in the levels of neutrophils, similar to the decrease observed in the MSU model. It is likely that the decrease in CXCL-1 (equivalent to human IL-8) could account for the lower numbers of neutrophils, as it is consistent with the known IL-8 induction in human airway goblet cells by IL-33 (ref. [41]). Thus, decreasing airway inflammation by inhibition of both IL-1- and IL-33-induced IL-8 production, could be more effective than IL-33 blockade alone in allergic asthma, supporting IL-1R3 blockade. Consistent with these observations was a significant improvement of airway resistance to MCh challenge, revealing clear functional consequences of the anti-inflammatory intervention.

The IMQ model is similarly dependent not only on IL-36, but also on IL-1 and IL-8, making this disease similarly attractive for IL-1R3 blockade[24,42,43]. In our study, MAB-mR3 significantly attenuated visual signs of the disease, that is disease severity. And like the previously observed reduction of neutrophils by MAB-mR3, we also observed significantly lower numbers of circulating neutrophils as well as decreased levels of the neutrophil activation marker, MPO, in the skin. In fact, visual scoring correlated to levels of skin MPO. Remarkably there was a highly significant reduction of both IL-17a, IL-17f and IL-22 expression. These cytokines each possess an important role in the pathogenesis of psoriasis[44], particularly for IL-22 where human mast cells produce large amounts of IL-22[45]. The observation that IL-1R3 blockade can inhibit the transcription of these cytokines supports a role for IL-1R3 targeting in psoriasis.

Although IL-1R3 is the co-receptor for ligand binding receptors of six different cytokines, IL-1R3 is not the only co-receptor shared by multiple cytokines. In fact, both the common γ chain (IL-2Rγ) and glycoprotein 130 (gp130 or IL-6ST (signal transducer)) are also required for the signaling of multiple cytokines. However, mice deficient of IL-2Rγ or gp130 have developmental abnormalities such as leukocyte production (IL-2Rγ) and organ development (gp130), respectively[46,47]. In contrast, IL-1R3-deficient mice display no signs of anatomic abnormalities and remain fully fertile[48]. Still,

suppressing multiple signaling pathways could reduce the potential to mount an innate immune response, increasing frequencies of infections and impacting the development of helper T cells, such as T_H1, T_H2 and T_H17. However, compared to using monotherapy such as anti-IL-33, using a lower dose of anti-IL-1R3 could still allow for a basic level of signaling through the primary pathways and remain disease suppressive. Considering the synergism between cytokines of the IL-1 family, reducing signaling in this family by IL-1R3 blockade, could more easily revert a vicious cycle, than intervening in multiple unrelated pathways. Thus, future research needs to address these concerns and considerations.

In summary, blocking IL-1R3 is a therapy to limit activities from six members of the IL-1 family. With a broad applicability and specific targeting, this offers a feasible treatment option with an extensive therapeutic range.

Online content

Any methods, additional references, Nature Research reporting summaries, source data, statements of code and data availability and associated accession codes are available at https://doi.org/10.1038/s41590-019-0467-1.

Received: 1 February 2018; Accepted: 12 July 2019;
Published online: 19 August 2019

References

1. Kopf, M., Bachmann, M. F. & Marsland, B. J. Averting inflammation by targeting the cytokine environment. *Nat. Rev. Drug Discovery* **9**, 703–718 (2010).
2. Lappalainen, U., Whitsett, J. A., Wert, S. E., Tichelaar, J. W. & Bry, K. Interleukin-1β causes pulmonary inflammation, emphysema, and airway remodeling in the adult murine lung. *Am. J.Respir. Cell Mol. Biol.* **32**, 311–318 (2005).
3. Prefontaine, D. et al. Increased expression of IL-33 in severe asthma: evidence of expression by airway smooth muscle cells. *J. Immunol.* **183**, 5094–5103 (2009).
4. Towne, J. E. & Sims, J. E. IL-36 in psoriasis. *Curr. Opin. Pharmacol.* **12**, 486–490 (2012).
5. Tortola, L. et al. Psoriasiform dermatitis is driven by IL-36-mediated DC-keratinocyte crosstalk. *J. Clin. Invest.* **122**, 3965–3976 (2012).
6. Garlanda, C., Dinarello, C. A. & Mantovani, A. The interleukin-1 family: back to the future. *Immunity* **39**, 1003–1018 (2013).
7. Boraschi, D. & Tagliabue, A. The interleukin-1 receptor family. *Semin. Immunol.* **25**, 394–407 (2013).
8. Wesche, H. et al. The interleukin-1 receptor accessory protein (IL-1RAcP) is essential for IL-1-induced activation of interleukin-1 receptor-associated kinase (IRAK) and stress-activated protein kinases (SAP kinases). *J. Biol. Chem.* **272**, 7727–7731 (1997).
9. Korherr, C., Hofmeister, R., Wesche, H. & Falk, W. A critical role for interleukin-1 receptor accessory protein in interleukin-1 signaling. *Eur. J. Immunol.* **27**, 262–267 (1997).
10. Hezareh, M., Hessell, A. J., Jensen, R. C., van de Winkel, J. G. & Parren, P. W. Effector function activities of a panel of mutants of a broadly neutralizing antibody against human immunodeficiency virus type 1. *J. Virol.* **75**, 12161–12168 (2001).
11. Leabman, M. K. et al. Effects of altered FcgammaR binding on antibody pharmacokinetics in cynomolgus monkeys. *MAbs* **5**, 896–903 (2013).
12. Hansel, T. T., Kropshofer, H., Singer, T., Mitchell, J. A. & George, A. J. The safety and side effects of monoclonal antibodies. *Nat. Rev. Drug Discovery* **9**, 325–338 (2010).
13. Lee, D. W. et al. Current concepts in the diagnosis and management of cytokine release syndrome. *Blood* **124**, 188–195 (2014).
14. Smith, D. E. et al. The soluble form of IL-1 receptor accessory protein enhances the ability of soluble type II IL-1 receptor to inhibit IL-1 action. *Immunity* **18**, 87–96 (2003).
15. Ter Horst, R. et al. Host and environmental factors influencing individual human cytokine responses. *Cell* **167**, 1111–1124 e1113 (2016).
16. Gantner, B. N., Simmons, R. M., Canavera, S. J., Akira, S. & Underhill, D. M. Collaborative induction of inflammatory responses by dectin-1 and Toll-like receptor 2. *J. Exp. Med.* **197**, 1107–1117 (2003).
17. Gow, N. A. et al. Immune recognition of *Candida albicans* beta-glucan by dectin-1. *J. Infect. Dis.* **196**, 1565–1571 (2007).
18. Martinon, F., Petrilli, V., Mayor, A., Tardivel, A. & Tschopp, J. Gout-associated uric acid crystals activate the NALP3 inflammasome. *Nature* **440**, 237–241 (2006).
19. Busso, N. & So, A. Mechanisms of inflammation in gout. *Arthritis Res. Ther.* **12**, 206 (2010).
20. Joosten, L. A. et al. Engagement of fatty acids with Toll-like receptor 2 drives interleukin-1beta production via the ASC/caspase 1 pathway in monosodium urate monohydrate crystal-induced gouty arthritis. *Arthritis Rheum.* **62**, 3237–3248 (2010).
21. Pham, C. T. Neutrophil serine proteases: specific regulators of inflammation. *Nat. Rev. Immunol.* **6**, 541–550 (2006).
22. Kakimoto, K., Matsukawa, A., Yoshinaga, M. & Nakamura, H. Suppressive effect of a neutrophil elastase inhibitor on the development of collagen-induced arthritis. *Cell Immunol.* **165**, 26–32 (1995).
23. Lee, H. Y. et al. Blockade of IL-33/ST2 ameliorates airway inflammation in a murine model of allergic asthma. *Exp. Lung Res.* **40**, 66–76 (2014).
24. Marrakchi, S. et al. Interleukin-36-receptor antagonist deficiency and generalized pustular psoriasis. *N. Engl J. Med.* **365**, 620–628 (2011).
25. Rossi-Semerano, L. et al. First clinical description of an infant with interleukin-36-receptor antagonist deficiency successfully treated with anakinra. *Pediatrics* **132**, e1043–e1047 (2013).
26. Flutter, B. & Nestle, F. O. TLRs to cytokines: mechanistic insights from the imiquimod mouse model of psoriasis. *Eur. J. Immunol.* **43**, 3138–3146 (2013).
27. Libby, P. Inflammation in atherosclerosis. *Arterioscler. Thromb. Vasc. Biol.* **32**, 2045–2051 (2012).
28. Grivennikov, S. I., Greten, F. R. & Karin, M. Immunity, inflammation, and cancer. *Cell* **140**, 883–899 (2010).
29. Ramanan, V. K. et al. GWAS of longitudinal amyloid accumulation on 18F-florbetapir PET in Alzheimer's disease implicates microglial activation gene IL1RAP. *Brain* **138**, 3076–3088 (2015).
30. Jaras, M. et al. Isolation and killing of candidate chronic myeloid leukemia stem cells by antibody targeting of IL-1 receptor accessory protein. *Proc. Natl Acad. Sci. USA* **107**, 16280–16285 (2010).
31. Ridker, P. M. et al. Antiinflammatory therapy with canakinumab for atherosclerotic disease. *N. Engl J. Med.* **377**, 1119–1131 (2017).
32. Ridker, P. M. et al. Effect of interleukin-1beta inhibition with canakinumab on incident lung cancer in patients with atherosclerosis: exploratory results from a randomised, double-blind, placebo-controlled trial. *Lancet* **390**, 1833–1842 (2017).
33. Bertheloot, D. & Latz, E. HMGB1, IL-1alpha, IL-33 and S100 proteins: dual-function alarmins. *Cell Mol. Immunol.* **14**, 43–64 (2017).
34. Hueber, A. J. et al. IL-33 induces skin inflammation with mast cell and neutrophil activation. *Eur. J. Immunol.* **41**, 2229–2237 (2011).
35. Enoksson, M. et al. Intraperitoneal influx of neutrophils in response to IL-33 is mast cell-dependent. *Blood* **121**, 530–536 (2013).
36. Afonina, I. S., Muller, C., Martin, S. J. & Beyaert, R. Proteolytic processing of interleukin-1 family cytokines: Variations on a common theme. *Immunity* **42**, 991–1004 (2015).
37. Guma, M. et al. Caspase 1-independent activation of interleukin-1beta in neutrophil-predominant inflammation. *Arthritis Rheum.* **60**, 3642–3650 (2009).
38. Nakae, S. et al. IL-1 is required for allergen-specific Th2 cell activation and the development of airway hypersensitivity response. *Int. Immunol.* **15**, 483–490 (2003).
39. Rabeony, H. et al. IMQ-induced skin inflammation in mice is dependent on IL-1R1 and MyD88 signaling but independent of the NLRP3 inflammasome. *Eur. J. Immunol.* **45**, 2847–2857 (2015).
40. Possa, S. S., Leick, E. A., Prado, C. M., Martins, M. A. & Tiberio, I. F. Eosinophilic inflammation in allergic asthma. *Front. Pharmacol.* **4**, 46 (2013).
41. Tanabe, T., Shimokawaji, T., Kanoh, S. & Rubin, B. K. IL-33 stimulates CXCL8/IL-8 secretion in goblet cells but not normally differentiated airway cells. *Clin. Exp. Allergy* **44**, 540–552 (2014).
42. Alvarez, P. & Jensen, L. E. Imiquimod treatment causes systemic disease in mice resembling generalized pustular psoriasis in an IL-1 and IL-36 dependent manner. *Mediators Inflamm.* **2016**, 6756138 (2016).
43. Sticherling, M., Sautier, W., Schroder, J. M. & Christophers, E. Interleukin-8 plays its role at local level in psoriasis vulgaris. *Acta Derm. Venereol.* **79**, 4–8 (1999).
44. Hawkes, J. E., Chan, T. C. & Krueger, J. G. Psoriasis pathogenesis and the development of novel targeted immune therapies. *J. Allergy Clin. Immunol.* **140**, 645–653 (2017).
45. Mashiko, S. et al. Human mast cells are major IL-22 producers in patients with psoriasis and atopic dermatitis. *J. Allergy Clin. Immunol.* **136**, 351–359 e351 (2015).
46. Betz, U. A. et al. Postnatally induced inactivation of gp130 in mice results in neurological, cardiac, hematopoietic, immunological, hepatic, and pulmonary defects. *J. Exp. Med.* **188**, 1955–1965 (1998).
47. Cao, X. et al. Defective lymphoid development in mice lacking expression of the common cytokine receptor gamma chain. *Immunity* **2**, 223–238 (1995).
48. Cullinan, E. B. et al. IL-1 receptor accessory protein is an essential component of the IL-1 receptor. *J. Immunol.* **161**, 5614–5620 (1998).

Acknowledgements

We thank J. Domenico and M. Wade for their technical assistance, and S.H. Kim (Laboratory of Cytokine Immunology, Konkuk Univ., Republic of Korea) and M. Fujita for providing cell lines. We thank the OLAR Vivarium, the ClinImmune Flow Core Facility and the Histology Shared Resource Center funded by the University of Colorado Cancer Center NIH grant (no. P30CA046934) at the University of Colorado Anschutz Medical Campus. We also thank the University of Colorado School of Medicine Biological Mass Spectrometry Facility for analyzing IP samples. J.F.H. was supported by the Oticon Foundation, Lundbeck Foundation, Knud Højgaard Foundation and the Interleukin Foundation. M.L.V.K and B.J.S. was supported by the Interleukin Foundation. A.S.M. was funded by NIH grants no. HL126736, ES025534 and HL135872-01. C.A.D. was funded by NIH grant no. AI-15614.

Author contributions

J.F.H. designed and performed experiments, analyzed data and wrote the manuscript. M.L.V.K. designed and performed experiments and analyzed data and assisted with manuscript preparation. A.S.M. and M.T.W. designed and performed experiments and analyzed data. T.A., L.P.L, D.M.D.G., B.J.S. and M.W. performed experiments and analyzed data. M.T. assisted in the experimental design and manuscript preparation. K.B. designed experiments and analyzed data. M.F. designed and supervised experiments and analyzed data. S.F. produced the human and mouse anti-IL-1R3 antibodies, designed experiments and analyzed data. C.A.D. designed experiments, analyzed data and edited the manuscript. All authors read and accepted the final manuscript.

Competing interests

K.B. is employed by MAB Discovery GmbH, Neuried, Germany. S.F. is the CEO of MAB Discovery GmbH. All other authors declare no competing interests.

Additional information

Supplementary information is available for this paper at https://doi.org/10.1038/s41590-019-0467-1.

Reprints and permissions information is available at www.nature.com/reprints.

Correspondence and requests for materials should be addressed to C.A.D.

Peer review information: Zoltan Fehervari was the primary editor on this article and managed its editorial process and peer review in collaboration with the rest of the editorial team.

Publisher's note: Springer Nature remains neutral with regard to jurisdictional claims in published maps and institutional affiliations.

Methods

Monoclonal antibody production and test of affinity. Human recombinant protein was used as the immunogen for wild-type albino zika rabbit immunization, whereafter the isolated and modified humanized IgG1 monoclonal Fc-LALA substituted IL-1R3 antibody (MAB-hR3) was produced in HEK293-FreeStyle cells (ThermoFisher Scientific). The antibody was purified from the supernatant using protein-A affinity chromatography followed by size exclusion chromatography (MAB Discovery GmbH). The mouse monoclonal chimeric IgG2a Fc-LALA substituted IL-1R3 antibody (MAB-mR3) was similarly produced (MAB Discovery GmbH) but used a specific mouse recombinant protein in an independent immunization campaign.

For both antibodies, the binding characteristics were determined using surface plasmon resonance (Biacore T200) carried out by an external provider (Biaffin GmbH & Co KG). Single-cycle set-ups were performed using increasing concentrations of human (0.111–9 nM or mouse (0.185–15 nM) IL-1R3, measuring the interaction with captured MAB-hR3 or MAB-mR3 respectively. Two independent measurements were performed for each tested antibody.

Functional testing of MAB-hR3. Cell-binding analyses of MAB-hR3 were carried out using NIH-3T3 (DMEM, 10% FCS) (ATCC) and SK-MEL-30 (RPMI, 10% FCS) cell lines. Cells were harvested using Accumax (Sigma), washed and resuspended in stain buffer (BD Pharmingen), before incubating with MAB-hR3 (10 μg ml^{-1}) or human IgG isotype control (MAB Discovery) for 30 min (4 °C). For EC_{50} and affinity calculations of SK-MEL-30 cell binding, cells were incubated in a 1:2 dilution series with MAB-hR3 starting at 20 μg ml^{-1}. Cells were subsequently washed with stain buffer and incubated with Alexa-488-labeled goat-anti-human secondary antibody (Dianova) for 30 min (4 °C). Afterwards, the cells were washed with staining buffer and resuspended in buffer containing 1:100 diluted DRAQ7 (Abcam) dead cell stain. Samples were run on an Accuri C6 Sampler and analyzed using FlowJo (ThreeStar).

Immunoprecipitation was performed according to the protocol using Dynabeads (Co-Immunoprecipitation kit; Life Technologies) coupled with MAB-hR3 (30 mg of Ab per milligram of beads) or human IgG isotype control (30 mg of Ab per milligram of beads; R&D Systems). A549 cells (ATCC) were stimulated in T175 flasks with recombinant human IL-1α (5 ng ml^{-1} for 15 min; Peprotech) to allow the cytokine-associated signaling complex to form (IL-1R1 + IL-1α + IL-1R3). Cells were then lysed (1× IP buffer from kit, 100 mM NaCl and protease inhibitor (1× Halt protease inhibitor cocktail; ThermoFisher scientific)) and the lysate was divided equally and incubated (30 min at 4 °C) with either MAB-hR3 or IgG-coupled beads (7.5 mg), followed by three washing steps.

The bound protein from the beads was eluted in buffer (0.5 M NH_4OH (14.8 N) and 0.5 mM EDTA) and lyophilized in a centrifugal vacuum concentrator for 6 h. Lyophilized proteins were solubilized in sample buffer (40% glycerol, 0.3 M Tris, 0.3 M SDS, 0.2 M dithiothreitol and 0.6 mM bromophenol blue in H_20) and heated at 37 °C (30 min) to avoid membrane protein aggregation. The samples were run on a 7.5% Mini-Protean TGX gel (BioRad).

The gels were stained with colloidal Coomassie[49] and visible bands including inbetween areas were excised and sent to the University of Colorado School of Medicine biological mass spectrometry facility for analysis. Here, gel pieces were destained (200 μl of 25 mM ammonium bicarbonate in 50 % (v/v) acetonitrile for 15 min) and washed twice (200 μl of 50% (v/v) acetonitrile). The disulfide bonds in proteins were reduced by incubation in 10 mM dithiothreitol at 60 °C for 30 min and cysteine residues were alkylated with 20 mM iodoacetamide in the dark (room temperature for 45 min). Gel pieces were subsequently washed with 100 μl of distilled water, followed by addition of 100 μl of acetonitrile and dried on SpeedVac (Savant ThermoFisher). Next, trypsin (100 ng) was added to each sample and allowed to rehydrate the gel plugs at 4 °C for 45 min, after which they were incubated at 37 °C overnight. The tryptic mixtures were acidified with formic acid up to a final concentration of 1%.

Peptides were extracted two times from the gel plugs using 1% formic acid in 50% acetonitrile. The collected extractions were pooled with the initial digestion supernatant and dried on SpeedVac (Savant ThermoFisher). Samples were then analyzed on an LTQ Orbitrap Velos mass spectrometer (ThermoFisher Scientific). This was coupled to an Eksigent nanoLC-2D system through a nanoelectrospray liquid chromatography–mass spectrometry interface as previously described[50]. We received a final report for the samples analyzed.

MAB-hR3 LALA substitution, PBMC viability and spontaneous cytokine production. To test the activity of IgG1 and IgG1-LALA versions of humanized anti-IL-1R3 in eliciting Fc-mediated effector cell functions such as ADCC, MAB-hR3 was tested both with and without an incorporated LALA substitution. We used a bioassay measuring the antibody-induced activity of a gene reporter (NFAT) in FcγRIIIa expressing Jurkat effector cells, thus, not a classical ADCC assay. Briefly, hIL-1R3-expressing target cells, SK-MEL-30 cells, were seeded in a 384-well tissue-culture-treated plate at a density of 2,500 cells per well in 25 μl RPMI medium containing 10% FCS. 24 h after seeding, 4,000 effector cells per well (ADCC Bioassay Effector cells, Jurkat, Promega) were added in RPMI medium containing 4% low-IgG-FCS. Antibodies were then added to a final concentration ranging from 0.002–10,000 ng ml^{-1}, and the plate was incubated for 6 h at 37 °C with 5% CO_2. Activation of NFAT signaling in luciferase gene-reporter Jurkat cells was measured according to the manufacturer's instructions (Bio-Glo luciferase assay) using a Tecan M1000 microplate reader.

Next, we evaluated the impact of MAB-hR3 on PBMCs using a conventional MTT reduction assay (Roche). PBMCs (500,000 per well) from three healthy donors were incubated with either medium or MAB-hR3 (1 μg ml^{-1} or 20 μg ml^{-1}). For the 24-h experiments, we used 96-well flat-bottomed plates without FCS in the medium, and for the 3- and 5-d experiments, we used round bottom wells with 10% FCS in the medium. The cells were assayed in triplicate after 24 h, 3d or 5 d. On the day of analysis, PBMCs were incubated for 2 h with MTT (20 μl in 200 μl) before adding MTT solvent for 15 min and measuring absorbance at 570 nm on an ELISA reader. Using the linearity between absorbance and viable cells converting MTT, we calculated the number of viable cells using medium alone as the control set to 100%. At same day of MTT analysis, we also harvested supernatants from PBMCs incubated under same conditions and from same donors, subsequently assaying for IL-6 production.

Cell line experiments. An A549 (NF-κB) luciferase reporter cell line (Signosis; DMEM, 10% FCS) (37 °C and 5% CO_2) was used for IL-1R1 investigation. Cells were seeded in 384-well flat-bottomed plates (40,000 cells per well), rested for 16 h before preincubating for 1 h with MAB-hR3 or polyclonal (goat-anti-human-IL-1R3; R&D Systems) antibody at increasing concentrations. Recombinant human IL-1α (0.1 ng ml^{-1}; R&D Systems) was added for 5 h. Steady-Glo (Promega) solution was used on lysates for development and luminescence was measured using a Tecan M1000 plate reader. The A549 cell line (ATCC) was cultured in T75 flasks (37 °C with 5% CO_2) in complete F-12K media (10% FCS). Cells were seeded in 96-well flat-bottomed plates (50,000 per well) and rested for 3 h before preincubating for 1 h with MAB-hR3 (1–20 μg ml^{-1}) or IL-1Ra (10 μg ml^{-1}). Cells were stimulated with recombinant human IL-1α (50 pg ml^{-1}; Peprotech) for 24 h and assayed for IL-6 production.

Inhibition of signaling through IL-1R4 was investigated using HEK-Blue SEAP reporter IL-33 cell line (NF-κB/AP-1 activation) (InvivoGen) (DMEM and 10% FCS at 37 °C with 5% CO_2). Cells were seeded in 384-well flat-bottomed plates (25,000 cells per well), rested for 16 h before preincubating for 1 h with MAB-hR3 or polyclonal (goat-anti-human-IL-1R3; R&D Systems) antibody at increasing concentrations. Recombinant human IL-33 (5 ng ml^{-1}; R&D Systems) was added and plates were incubated overnight. Supernatants were transferred to clear, flat-bottomed polystyrene NBS microplates (Corning) containing 2× QUANTI-Blue reagent (InvivoGen) and incubated (37 °C for 45 min) before measuring the optical density (655 nm) using a Tecan M1000 plate reader. The human mast cell line (HMC-1) was used to investigate the impact on IL-33-induced IL-8 production. The cell line was cultured in T75 flasks (37 °C with 5% CO_2) in complete Iscove's modified Dulbecco's medium (10% FCS and 1% penicillin/streptomycin). HMC-1 cells were seeded in 96-well flat-bottomed plates (50,000 per well) and rested for 3 h before preincubating for 1 h with MAB-hR3 (1–20 μg ml^{-1}) or IL-1Ra (10 μg ml^{-1}). Cells were stimulated with recombinant human IL-33 (20 ng ml^{-1}; R&D Systems) for 24 h and assayed for IL-8 production.

Inhibition of signaling through IL-1R6 was investigated using a HEK293/17 luciferase reporter cell line (NF-κB activation) (MAB Discovery GmbH; DMEM, 10 % FCS, 20 μg ml^{-1} hygromycin at 37 °C with 5% CO_2). Cells were seeded in 384-well flat-bottomed plates (30,000 per well) and rested for 16 h before preincubating for 1 h with MAB-hR3 or polyclonal (goat-anti-human-IL-1R3; R&D Systems) antibody at increasing concentrations. Recombinant human IL-36γ (15 ng ml^{-1}; R&D Systems) was added and incubated for 5 h. Steady-Glo (Promega) solution was used on lysates for development, and luminescence was measured using a Tecan M1000 plate reader. The impact on IL-36-induced IL-8 production was investigated using a human keratinocytic cell line (HaCaT). The cell line was cultured in T75 flasks (37 °C with 5% CO_2) in complete DMEM (10% FCS). HaCaT cells were seeded in 96-well flat-bottomed plates (50,000 per well) and rested for 3 h before preincubating 1 h with MAB-hR3 (1–20 μg ml^{-1}) or IL-1Ra (10 μg ml^{-1}). Cells were stimulated with recombinant human IL-36α (50 ng ml^{-1}; R&D Systems) for 24 h and assayed for IL-8 production.

Cytokine production in whole-blood reactions with soluble IL-1R3. Using freshly obtained blood collected in heparin tubes, 250 μl was preincubated with 550 μl RPMI (no FCS) and 100 μl of inhibitor (media, MAB-hR3 or IL-1Ra). After 1 h, 100 μl of stimulant was added using medium or heat-killed *C. albicans* (0.5×10^6 ml^{-1})[51]. After 24 h of incubation, supernatants were harvested and analyzed for sIL-1R1, sIL-1R2, sIL-1R3, sIL-1R4, IL-6 or IL-17 production. For sIL-1R3 investigation, we used recombinant human IL-1R3 protein (R&D Systems). To test for binding to MAB-hR3, we preincubated (14 h) MAB-hR3 (1 μg ml^{-1}) with sIL-1R3 (62.5–1,000 ng ml^{-1}) before adding 100 μl of this mix to the heat-killed *C. albicans* stimulations as the inhibitor. To investigate the anti-inflammatory effect of sIL-1R3 alone, we used increasing concentrations (62.5–1,000 ng ml^{-1}) of sIL-1R3 without MAB-hR3 as an inhibitor in the set-up.

Functional testing of anti-mouse IL-1R3 (MAB-mR3) and comparison to MAB-hR3. The functionality of MAB-mR3 was tested in murine NIH-3T3 (NF-κB) luciferase reporter cell lines (Signosis; DMEM and 10% FCS) seeded in

384-well flat-bottomed plates (20,000 cells per well (30,000 cells per well for IL-33 stimulations)) and rested for 16 h (37 °C with 5% CO_2) before preincubating 1 h with MAB-mR3 antibody at increasing concentrations. Recombinant mIL-1β (50 pg ml^{-1}), mIL-33 (1 ng ml^{-1}) or mIL-36γ (170 ng ml^{-1}) (R&D Systems) was added and plates incubated for 5 h (37 °C with 5% CO_2). Steady-Glo (Promega) solution was used on lysates and luminescence was measured (Tecan M1000 plate reader). Inhibition of IL-6 release was determined in a NIH-3T3 cell line (ATCC), seeded in 384-well flat-bottomed plates (12,500 cells per well) and rested for 2 h (37 °C with 5% CO_2) before preincubating for 1 h with MAB-mR3 or MAB-hR3 antibody at increasing concentrations. Cells were stimulated with recombinant hIL-1β (50 pg ml^{-1}, R&D Systems) for 16 h and assayed for IL-6 production.

Monosodium urate crystal peritonitis model. MAB-mR3 was administered to wild-type 8-week-old C57BL/6J male mice (Jackson Laboratories). MSU crystal-induced peritonitis was induced with 3 mg of MSU (diluted in 200 µl PBS; Invivogen) per mouse by IP injection. MAB-mR3 (500 µg per mouse (17.2 µM), MAB Discovery) was compared to IL-1Ra (anakinra, 10 mg kg^{-1} (232 µg per mouse (67.1 µM)) as the inhibitor (200 µl per mouse). The four groups were comprised of: saline as vehicle control for MSU and inhibitor ($n=4$), MSU alone with saline as inhibitor ($n=8$), MSU with MAB-mR3 ($n=8$) and the last group with MSU and IL-1Ra ($n=8$). Each intervention group was represented by at least one mouse in each cage. MAB-mR3, IL-1Ra or saline was injected IP 1 h before MSU stimulation. The mice were euthanized 6 h after MSU or saline injection. Blood was collected in microcentrifuge tubes containing EDTA and peritoneal fluid was collected by lavage using 10 ml of ice-cold PBS. Organs were immediately frozen in liquid nitrogen. Plasma and whole-blood lysate (TritonX 0.5%) were assayed for cytokines. The differential number of cells collected by centrifugation (300*g* for 10 min) of IP fluid was counted (HESKA HemaTrue) and lysed (TritonX 0.5%). Cytokines were measured in both the IP fluid and IP cell lysates. For low abundance cytokines in the IP fluid, 8 ml of fluid was concentrated (end range, 4.7–10.9× concentrated) in preboiled (15 min) dialysis membranes (MWCO 3.5 kDa, Spectra/Por3 dialysis membrane; Spectrumlabs) submerged in polyethylene glycol (MN 6-8000; Sigma-Aldrich) as the hygroscopic solution (4 °C). Initial concentrations were calculated by dividing with the dialysis concentration factor. Spleen lysates were assayed for cytokine levels and normalized to protein concentration of the lysates. Protein levels in spleen lysates and IP fluid were assayed with a standard Bradford assay, using protein assay dye reagent (BioRad) and BSA as a standard.

PBMC stimulations and mixed leukocyte reactions. For PBMC stimulations, we used 500,000 freshly isolated PBMCs per well in 96-well round-bottomed plates at a total volume of 200 µl. Cells were seeded and incubated with either medium alone, MAB-hR3 (69 nM (10 µg ml^{-1})), sIL-1R4 ((69 nM (4.3 µg ml^{-1})) (R&D Systems), IL-36Ra (69 nM (1.2 µg ml^{-1})) (R&D Systems) or IL-1Ra (587 nM (10 µg ml^{-1})) for 1 h before stimulation. PBMCs were then stimulated with heat-killed *C. albicans* (0.5×10^6 microorganisms ml^{-1}, for 5 d in RPMI and 10% FCS). After stimulation, supernatants were harvested and assayed for cytokine production.

In two-way MLRs, we combined freshly isolated PBMCs from two unrelated healthy donors. PBMCs were mixed in a 1:1 ratio in 96-well round-bottomed plates (250,000 cells per donor at 200 µl final volume) and incubated for 5 d (RPMI and 10% FCS) with either medium alone, MAB-hR3 (5–20 µg ml^{-1}) or IL-1Ra (10 µg ml^{-1}). Cytokine production was measured in the supernatants using both the Quansys multiplex platform and ELISA (Duoset, R&D Systems).

Ovalbumin allergic airway inflammation model. For the first OVA experiment (exp.1), we used wild-type 6-week-old C57BL/6J male mice (Jackson Laboratories), sensitized IP using OVA (15 µg 100 µl^{-1}; Sigma-Aldrich) mixed 1:1 with Imject Alum Adjuvant (100 µl; ThermoFisher). In the second experiment (exp. 2), we similarly used wild-type 6-week-old C57BL/6J male mice (Jackson Laboratories) but sensitized them using a lower concentration of OVA (10 µg 100 µl^{-1}, Sigma-Aldrich) mixed 1:1 with Imject Alum Adjuvant (100 µl; ThermoFisher). For exp. 1 and exp. 2, mice were injected at day 1, 14 and 21. Around day 25–28, mice were injected IP with MAB-mR3 (500 µg per mouse; MAB Discovery) or mouse IgG control (500 µg per mouse; MAB Discovery).

For exp.1, intratracheal instillation of OVA (50 µg per mouse in 50 µl) was performed 30 min after injection at around day 26–28 in short-term CO_2 anesthesia. Exp. 2 used aerosolized OVA (1% w/v in PBS). BAL was carried out as previously described by inserting a catheter into the trachea and washing the airways with 3 × 1 ml washes[52]. BAL cells were enumerated by trypan blue exclusion. This was followed by cell phenotyping using flow cytometry (exp.1) or cytospined and stained with Diff-Quick (DADE Diagnostics) (exp. 2). The following mAbs against mouse targets were used for flow cytometry following mouse Fc Block (BD Biosciences): PE-Cy7 CD11c (N418), PerCP-Cy5.5 CD11b (M1/70), FITC-Ly6G (1A8-Ly6G) (all eBioscience); PE-Siglec-F (E250-4440) (from BD Biosciences) (1:400 dilution for all mAbs; stained in DPBS containing 10 mg ml^{-1} of BSA and 0.1 mg ml^{-1} of NaN_3) (Gating strategy in supplementary Fig. 3). Cells were analyzed on a Canto II flow cytometer using FlowJo software (Treestar). Following BAL, the lungs were standard inflated with 4% PFA for 20 min with a pressure of 20 cm water column and subsequently stored in formalin overnight. Afterwards, lungs were embedded in agarose and cut in 2-mm thick slices according to the orientator principle. Lung slices were embedded in paraffin, sectioned and stained with H&E or PAS. Histology was evaluated using an Olympus DP-25 digital camera, connected to a BX-51 (Olympus) microscope using 40-fold and 100-fold magnifications (Olympus Cell A software). The area of mucin-containing goblet cells was quantified as previously described[53], using systematic uniform random sampling[54,55]. Airway responsiveness to MCh was obtained using invasive lung function assessments (FinePointe RC Units, Data Sciences International) as previously described[53].

Imiquimod psoriasis model. Wild-type 12-week-old C57BL/6J male mice (Jackson Laboratories) were back-skin shaved and treated with hair removal cream (Nair). Application of 75 mg IMQ (Aldara 5% IMQ) or control cream (Vaseline cream) was done daily (days 1–5) on back skin (IMQ-receiving groups: IMQ group ($n=10$) and MAB-mR3 group ($n=9$) versus control cream-receiving group: vehicle group ($n=3$)). IP injections were given every other day (days 1, 3 and 5). The vehicle and untreated IMQ group received mouse IgG control (20 mg kg^{-1}; MAB Discovery). The IMQ treatment group received MAB-mR3 (20 mg kg^{-1}; MAB Discovery). Ears were concurrently applied with control cream on the left ear (all mice, 5 mg of Vaseline cream) and group-appropriate stimuli cream on the right ear (vehicle group, 5 mg of Vaseline cream; IMQ and MAB-mR3 groups, 5 mg IMQ cream).

Body weight and erythema development was monitored daily. Mice were euthanized on day 6, where left and right ear thickness was measured using an engineer's micrometer (Mitutoyo). Whole-blood cell counts were assessed using a HemaTrue analyzer (HESKA). Pictures of the back skin were visually scored (erythema and scaling, score 0 (no response) to 4 (maximum affected)) by six blinded people. RNA was isolated from skin puncture biopsies. Trizol (4 °C, Invitrogen) and a rotor stator homogenizer were used to lyse samples. RNA was extracted from lysates using RNeasy Mini spin columns (Qiagen) following the manufacturer's protocol. cDNA was produced from 0.8 µg RNA (NanoDrop; High Capacity cDNA Reverse Transcription kit (Applied Biosystems)). 50 ng cDNA was used in a 20 µl real-time qPCR reaction using SYBR Green master mix (Applied Biosystems) and 0.1 µM of IL-36α, IL-36β, IL-36γ, IL-17 A, IL-17F or IL-22 primers. The qPCRs were run on a BioRad CFX96 real-time PCR platform. Glyceraldehyde 3-phosphate dehydrogenase was used as a reference gene and ratios were calculated using the Pfaffl method, including analyzed primer efficiencies. We used the following primer sequences for mouse IL-36α (forward: 5′-ATCTGGACACTCTTGAGACG-3′, reverse: 3′-GAGAGGCTTTTACAGGTTCC-5′); mouse IL-36β (forward: 5′-CACTATGC ATGGATCCTCAC-3′, reverse: 3′-TGTCTCTACATGCTATCAAGC-5′); mouse IL-36γ (forward: 5′-ATGGACACCCTACTTTGCTG-3′, reverse: 5′-CAGGGTGGTGGTACAAATC-3′); mouse IL-17A (forward: 5′-TCCAG AAGGCCCTCAGACTA-3′, reverse: 3′-TCAGGACCAGGATCTCTTGC-5′); mouse IL-17 F (forward: 5′-CCATTCTGAGGGAGGTAGCA-3′, reverse: 3′-GGGGTCTCGAGTGATGTTGT-5′); mouse IL-22 (forward: 5′-TCA TCGGGGAGAAACTGTTC-3′, reverse: 3′-TCTGGATGTTCTGGTCGTCA-5′) and mouse glyceraldehyde 3-phosphate dehydrogenase (forward: 5′-TGCA CCACCAACTGCTTAGC-3′, reverse: 3′-GGCATGGACTGTGGTCATGAG-5′).

MPO levels were measured in a freshly obtained skin biopsy, homogenized in 1% TritonX 100 containing collagenase I and protease inhibitor (Complete Mini Tablet, Roche) using a rotor stator homogenizer. The lysate was spun at 12,000*g* (4 °C for 20 min) and supernatants were used for cytokine measurement by ELISA and measurements of protein levels by Bradford assay (BioRad), following the manufacturer's protocol. MPO was normalized to total protein in the sample.

Common procedures, background information and statistical analysis. Cytokine and soluble receptor concentrations were measured according to protocol using Duoset ELISA (R&D Systems) or multiplex assays (Quansys Biosciences). PBMCs for stimulations were freshly isolated (Histopaque-1077, Sigma-Aldrich) using heparin-containing tubes and washed three times with 0.9% saline before use. Cell lines were tested as mycoplasma-free before use. PBMCs were obtained from healthy donors after obtaining informed consent. The study was approved by the Colorado Multiple Institutional Review Board. All in vivo mouse models were approved by the University of Colorado Denver Animal Care and Use Committee or the Animal Research Ethics Board of the Ministry of Environment (Kiel, Germany).

Cell line IC_{50} values were calculated using an incorporated [inhibitor] versus response function in GraphPad Prism. Comparison between IC_{50} values was conducted using the extra-sum-of-squares F test. The binding affinity for cell lines was calculated using the binding kinetics function in Graphpad Prism, assuming complete specific binding. The impact of inhibitors on cell lines, PBMCs, whole-blood cultures and MLRs were evaluated using either a paired two-sided Student's *t*-test or a Wilcoxon signed-rank test, as appropriate. Multiple comparisons were evaluated using a Holm–Sidaks multiple comparisons test. Differences between groups in vivo were tested using a Mann–Whitney *U*-test or Student's *t*-test as appropriate. Two-tailed *P* values ≤0.05 were considered significant. GraphPad Prism v.7 (GraphPad software) was used for statistical analysis and graphical representations. For further information, see the Reporting Summary.

Reporting Summary. Further information on research design is available in the Nature Research Reporting Summary linked to this article.

Data availability

The data that support the findings of this study are available upon request to the corresponding author.

References

49. Dyballa, N. & Metzger, S. Fast and sensitive colloidal coomassie G-250 staining for proteins in polyacrylamide gels. *J. Vis. Exp.* **3**, 1431 (2009).
50. Moore, H. B. et al. Hemolysis exacerbates hyperfibrinolysis, whereas platelolysis shuts down fibrinolysis: evolving concepts of the spectrum of fibrinolysis in response to severe injury. *Shock* **43**, 39–46 (2015).
51. van de Veerdonk, F. L. et al. Protective host defense against disseminated candidiasis is impaired in mice expressing human interleukin-37. *Front. Microbiol.* **5**, 762 (2014).
52. McKee, A. S., Mack, D. G., Crawford, F. & Fontenot, A. P. MyD88 dependence of beryllium-induced dendritic cell trafficking and CD4(+) T-cell priming. *Mucosal Immunol.* **8**, 1237–1247 (2015).
53. Lunding, L. P. et al. Poly(inosinic-cytidylic) acid-triggered exacerbation of experimental asthma depends on IL-17A produced by NK cells. *J. Immunol.* **194**, 5615–5625 (2015).
54. Fehrenbach, H. et al. Ultrastructural pathology of the alveolar type II pneumocytes of human donor lungs. Electron microscopy, stereology, and microanalysis. *Virchows Arch.* **432**, 229–239 (1998).
55. Mattfeldt, T., Mall, G., Gharehbaghi, H. & Moller, P. Estimation of surface area and length with the orientator. *J. Microsc.* **159**, 301–317 (1990).

nature research

Corresponding author(s): Charles Dinarello

Last updated by author(s): Jul 9, 2019

Reporting Summary

Nature Research wishes to improve the reproducibility of the work that we publish. This form provides structure for consistency and transparency in reporting. For further information on Nature Research policies, see Authors & Referees and the Editorial Policy Checklist.

Statistics

For all statistical analyses, confirm that the following items are present in the figure legend, table legend, main text, or Methods section.

n/a	Confirmed	
☐	☒	The exact sample size (*n*) for each experimental group/condition, given as a discrete number and unit of measurement
☐	☒	A statement on whether measurements were taken from distinct samples or whether the same sample was measured repeatedly
☐	☒	The statistical test(s) used AND whether they are one- or two-sided *Only common tests should be described solely by name; describe more complex techniques in the Methods section.*
☐	☒	A description of all covariates tested
☐	☒	A description of any assumptions or corrections, such as tests of normality and adjustment for multiple comparisons
☐	☒	A full description of the statistical parameters including central tendency (e.g. means) or other basic estimates (e.g. regression coefficient) AND variation (e.g. standard deviation) or associated estimates of uncertainty (e.g. confidence intervals)
☐	☒	For null hypothesis testing, the test statistic (e.g. *F*, *t*, *r*) with confidence intervals, effect sizes, degrees of freedom and *P* value noted *Give P values as exact values whenever suitable.*
☒	☐	For Bayesian analysis, information on the choice of priors and Markov chain Monte Carlo settings
☒	☐	For hierarchical and complex designs, identification of the appropriate level for tests and full reporting of outcomes
☐	☒	Estimates of effect sizes (e.g. Cohen's *d*, Pearson's *r*), indicating how they were calculated

Our web collection on statistics for biologists contains articles on many of the points above.

Software and code

Policy information about availability of computer code

Data collection	FlowJo v10 and Olympus cell A software v3.4
Data analysis	Graphpad Prism v7, FlowJo v10 and Olympus cell A software v3.4

For manuscripts utilizing custom algorithms or software that are central to the research but not yet described in published literature, software must be made available to editors/reviewers. We strongly encourage code deposition in a community repository (e.g. GitHub). See the Nature Research guidelines for submitting code & software for further information.

Data

Policy information about availability of data

All manuscripts must include a data availability statement. This statement should provide the following information, where applicable:

- Accession codes, unique identifiers, or web links for publicly available datasets
- A list of figures that have associated raw data
- A description of any restrictions on data availability

The data that support the findings of this study are available upon request to the corresponding author.

Field-specific reporting

Please select the one below that is the best fit for your research. If you are not sure, read the appropriate sections before making your selection.

☒ Life sciences ☐ Behavioural & social sciences ☐ Ecological, evolutionary & environmental sciences

For a reference copy of the document with all sections, see nature.com/documents/nr-reporting-summary-flat.pdf

Life sciences study design

All studies must disclose on these points even when the disclosure is negative.

Sample size	Sample sizes were determined according to previous data published using similar stimuli and cytokine evaluation. Sample size of in vivo models, was carefully determined based on similar studies using similar models and outcome measures.
Data exclusions	No data were excluded from the analysis.
Replication	All experiments were either succesfully replicated when using cell lines, or included a sufficient sample size, taking into account the expected variability when using human PBMCs and mice. Representative data was confirmed at least once with an independent experiment.
Randomization	In vitro experiments were not randomized, but to adjust for covariates, same lot-numbers of materials were used. Healthy donors were randomly selected. Mice were randomly assigned to group specific interventions.
Blinding	Blinding was done for skin scoring of pictures in the IMQ-model. All other data aquisition and analysis was not blinded.

Reporting for specific materials, systems and methods

We require information from authors about some types of materials, experimental systems and methods used in many studies. Here, indicate whether each material, system or method listed is relevant to your study. If you are not sure if a list item applies to your research, read the appropriate section before selecting a response.

Materials & experimental systems

n/a	Involved in the study
☐	☒ Antibodies
☐	☒ Eukaryotic cell lines
☐	☐ Palaeontology
☐	☒ Animals and other organisms
☐	☒ Human research participants
☐	☐ Clinical data

Methods

n/a	Involved in the study
☐	☐ ChIP-seq
☐	☒ Flow cytometry
☐	☐ MRI-based neuroimaging

Antibodies

Antibodies used	Antibodies used for mouse BAL cell phenotyping: PE-Cy7 CD11c (N418)(Lot: 2005223, Cat: 25-0114-82), PerCP-Cy5.5 CD11b (M1/70)(Lot: 4332809, Cat: 45-0112-82), FITC-Ly6G (1A8-Ly6G) (Lot:, Cat: 11-9668-82) (all eBioscience)); PE-Siglec-F (E50-2440) (Lot: 7208832, Cat:552126 (from BD Biosciences). Antibodies used to block IL-1R3 signaling: A humanized IgG1 monoclona Fc-LALA mutated IL-1R3 antibody (MAB-hR3, MAB Discovery) and a mouse monoclonal chimeric IgG2a Fc-LALA mutated IL-1R3 antibody (MAB-mR3, MAB Discovery). Isotype controls were used for both antibodies (MAB Discovery). For cell binding analysis Alexa-488 labelled goat-anti-human 2nd antibody (Dianova) was similarly used.
Validation	Antibodies used for mouse BAL cell phenotyping were all from approved commercial sources, company validated for mouse cell phenotyping. All antibodies had been previously used in similar mouse experiments and titrated for optimal performance (dilution 1:400 for all). Antibodies used to block and control for IL-1R3 signaling were all produced and validated by MAB Discovery. 2nd antibody for cell binding analysis had been preciously used in the lab at similar experiments and from an approved commercial source.

Eukaryotic cell lines

Policy information about cell lines

Cell line source(s)	HEK-293 (Thermofischer), NIH-3T3 (ATCC), SK-MEL-30 (kindly provided by Prof. Mayumi Fujita), A549 (ATCC), A549 reporter (Signosis), HEK-Blue reporter (Invivogen), HMC-1 (kindly provided by Prof. SooHyun Kim), HEK-293/17 reporter (MAB Discovery), HaCaT (kindly provided by Prof. Mayumi Fujita), NIH-3T3 reporter (Signosis).
Authentication	None of the cell lines used has been authenticated.
Mycoplasma contamination	All cell lines tested negative for mycoplasma contamination.
Commonly misidentified lines (See ICLAC register)	No commonly misidentified cell lines were used.

Palaeontology

Specimen provenance	*Provide provenance information for specimens and describe permits that were obtained for the work (including the name of the issuing authority, the date of issue, and any identifying information).*
Specimen deposition	*Indicate where the specimens have been deposited to permit free access by other researchers.*
Dating methods	*If new dates are provided, describe how they were obtained (e.g. collection, storage, sample pretreatment and measurement), where they were obtained (i.e. lab name), the calibration program and the protocol for quality assurance OR state that no new dates are provided.*

☐ Tick this box to confirm that the raw and calibrated dates are available in the paper or in Supplementary Information.

Animals and other organisms

Policy information about studies involving animals; ARRIVE guidelines recommended for reporting animal research

Laboratory animals	Wild-type 8weeks old C57BL/6J male mice (Jackson Laboratories) for MSU exp. Wild-type 6weeks old C57BL/6J male mice (Jackson Laboratories) for OVA experiments. Wild-type 12 weeks old C57BL/6J male mice (Jackson Laboratories) for IMQ exp.
Wild animals	The study did not involve wild animals.
Field-collected samples	The study did not involve samples collected from the field.
Ethics oversight	All in vivo mouse models were approved by the University of Colorado Denver Animal Care and Use Committee or the Animal Research Ethics Board of the Ministry of Environment (Kiel, Germany).

Note that full information on the approval of the study protocol must also be provided in the manuscript.

Human research participants

Policy information about studies involving human research participants

Population characteristics	Whole blood and PBMCs were obtained from healthy individuals including both women and men (age between 20-60).
Recruitment	Participants were recruited among university employees by asking them directly. The participants could be healthier than average, still this does not affect the conclusions to be made in this study.
Ethics oversight	The study was approved by the Colorado Multiple Institutional Review Board (COMIRB)

Note that full information on the approval of the study protocol must also be provided in the manuscript.

Clinical data

Policy information about clinical studies

All manuscripts should comply with the ICMJE guidelines for publication of clinical research and a completed CONSORT checklist must be included with all submissions.

Clinical trial registration	*Provide the trial registration number from ClinicalTrials.gov or an equivalent agency.*
Study protocol	*Note where the full trial protocol can be accessed OR if not available, explain why.*
Data collection	*Describe the settings and locales of data collection, noting the time periods of recruitment and data collection.*
Outcomes	*Describe how you pre-defined primary and secondary outcome measures and how you assessed these measures.*

ChIP-seq

Data deposition

☐ Confirm that both raw and final processed data have been deposited in a public database such as GEO.

☐ Confirm that you have deposited or provided access to graph files (e.g. BED files) for the called peaks.

Data access links *May remain private before publication.*	*For "Initial submission" or "Revised version" documents, provide reviewer access links. For your "Final submission" document, provide a link to the deposited data.*
Files in database submission	*Provide a list of all files available in the database submission.*
Genome browser session (e.g. UCSC)	

Provide a link to an anonymized genome browser session for "Initial submission" and "Revised version" documents only, to enable peer review. Write "no longer applicable" for "Final submission" documents.

Methodology

Replicates	*Describe the experimental replicates, specifying number, type and replicate agreement.*
Sequencing depth	*Describe the sequencing depth for each experiment, providing the total number of reads, uniquely mapped reads, length of reads and whether they were paired- or single-end.*
Antibodies	*Describe the antibodies used for the ChIP-seq experiments; as applicable, provide supplier name, catalog number, clone name, and lot number.*
Peak calling parameters	*Specify the command line program and parameters used for read mapping and peak calling, including the ChIP, control and index files used.*
Data quality	*Describe the methods used to ensure data quality in full detail, including how many peaks are at FDR 5% and above 5-fold enrichment.*
Software	*Describe the software used to collect and analyze the ChIP-seq data. For custom code that has been deposited into a community repository, provide accession details.*

Flow Cytometry

Plots

Confirm that:

☒ The axis labels state the marker and fluorochrome used (e.g. CD4-FITC).

☒ The axis scales are clearly visible. Include numbers along axes only for bottom left plot of group (a 'group' is an analysis of identical markers).

☒ All plots are contour plots with outliers or pseudocolor plots.

☒ A numerical value for number of cells or percentage (with statistics) is provided.

Methodology

Sample preparation	Cell binding analyses of MAB-hR3 were carried out using NIH-3T3 (DMEM, 10% FCS) (ATCC) and 643 SK-MEL-30 (RPMI, 10% FCS) (kindly provided by Prof. Mayumi Fujita) cell lines. Cells were harvested using Accumax (Sigma), washed and resuspended in stain buffer (BD Pharmingen), before incubating with MAB-hR3 (10 µg/mL) or human IgG isotype control (MAB Discovery) for 30min (4°C).Cells were subsequently washed with stain buffer and incubated with Alexa-488 labelled goat-anti-human secondary antibody (Dianova) for 30min (4°C). Afterwards, the cells were washed with staining buffer and resuspended in buffer containing 1:100 diluted DRAQ7 (Abcam) dead cell stain.
Instrument	Cell binding analyses were analyzed using an Accuri C6 Sampler, mouse BAL cell phenotyping were analyzed using a CANTO II Flow cytometer.
Software	FlowJo software v10 (Treestar) were used to collect and analyze data.
Cell population abundance	Cell binding analyses were done on single cell lines at a time with subsequent Live/dead staining (>97% live cells). Mouse BAL cell phenotyping was done on total collected live cells (>95%).
Gating strategy	For cell binding analyses we used FSC/SSC gating based on known morphology with subsequent Live/dead gating based on previous experiments. For mouse BAL cell phenotyping, we used singlet/FSC-SSC/live-dead gating before phenotypic gating based on antibody binding. Backgating were done to validate results. Phenotypic gating were kept consistent throughout.

☒ Tick this box to confirm that a figure exemplifying the gating strategy is provided in the Supplementary Information.

Magnetic resonance imaging

Experimental design

Design type	*Indicate task or resting state; event-related or block design.*
Design specifications	*Specify the number of blocks, trials or experimental units per session and/or subject, and specify the length of each trial or block (if trials are blocked) and interval between trials.*
Behavioral performance measures	*State number and/or type of variables recorded (e.g. correct button press, response time) and what statistics were used to establish that the subjects were performing the task as expected (e.g. mean, range, and/or standard deviation across subjects).*

Acquisition

Imaging type(s) *Specify: functional, structural, diffusion, perfusion.*

Field strength *Specify in Tesla*

Sequence & imaging parameters *Specify the pulse sequence type (gradient echo, spin echo, etc.), imaging type (EPI, spiral, etc.), field of view, matrix size, slice thickness, orientation and TE/TR/flip angle.*

Area of acquisition *State whether a whole brain scan was used OR define the area of acquisition, describing how the region was determined.*

Diffusion MRI ☐ Used ☐ Not used

Preprocessing

Preprocessing software *Provide detail on software version and revision number and on specific parameters (model/functions, brain extraction, segmentation, smoothing kernel size, etc.).*

Normalization *If data were normalized/standardized, describe the approach(es): specify linear or non-linear and define image types used for transformation OR indicate that data were not normalized and explain rationale for lack of normalization.*

Normalization template *Describe the template used for normalization/transformation, specifying subject space or group standardized space (e.g. original Talairach, MNI305, ICBM152) OR indicate that the data were not normalized.*

Noise and artifact removal *Describe your procedure(s) for artifact and structured noise removal, specifying motion parameters, tissue signals and physiological signals (heart rate, respiration).*

Volume censoring *Define your software and/or method and criteria for volume censoring, and state the extent of such censoring.*

Statistical modeling & inference

Model type and settings *Specify type (mass univariate, multivariate, RSA, predictive, etc.) and describe essential details of the model at the first and second levels (e.g. fixed, random or mixed effects; drift or auto-correlation).*

Effect(s) tested *Define precise effect in terms of the task or stimulus conditions instead of psychological concepts and indicate whether ANOVA or factorial designs were used.*

Specify type of analysis: ☐ Whole brain ☐ ROI-based ☐ Both

Statistic type for inference (See Eklund et al. 2016) *Specify voxel-wise or cluster-wise and report all relevant parameters for cluster-wise methods.*

Correction *Describe the type of correction and how it is obtained for multiple comparisons (e.g. FWE, FDR, permutation or Monte Carlo).*

Models & analysis

n/a	Involved in the study
☐	☐ Functional and/or effective connectivity
☐	☐ Graph analysis
☐	☐ Multivariate modeling or predictive analysis

Functional and/or effective connectivity *Report the measures of dependence used and the model details (e.g. Pearson correlation, partial correlation, mutual information).*

Graph analysis *Report the dependent variable and connectivity measure, specifying weighted graph or binarized graph, subject- or group-level, and the global and/or node summaries used (e.g. clustering coefficient, efficiency, etc.).*

Multivariate modeling and predictive analysis *Specify independent variables, features extraction and dimension reduction, model, training and evaluation metrics.*